

This manuscript has been submitted for publication
to *Geochimica et Cosmochimica Acta*

Please note that it has not been peer-reviewed at this stage!

If accepted, the final version of this manuscript will be available via the
Peer-reviewed Publication DOI link on the right-hand side of the EarthArXiv webpage.

Effects of mineralogy on Δ_{47} and Δ_{48} of carbonate-derived CO₂ below analytical resolution

Miguel Bernecker^{1, *}, Magali Bonifacie², Philip Staudigel¹, Niels Meijer³, Julien Siebert², Nicolas Wehr², Eiken Haussühl¹, Stefano M. Bernasconi⁴, Daniel Petrash⁵, Martin Dietzel⁶, Jens Fiebig¹

¹Institut für Geowissenschaften, Goethe-Universität Frankfurt, Altenhöferallee 1, 60438 Frankfurt am Main, Germany

²Université Paris Cité, Institut de Physique du Globe de Paris, CNRS, F-75005 Paris, France

³Senckenberg Biodiversität und Klima Forschungszentrum, Senckenberganlage 25, 60325 Frankfurt am Main, Germany

⁴Department of Earth and Planetary Sciences, ETH Zürich, Sonneggstrasse 5, 8092 Zürich, Switzerland

⁵Czech Geological Survey, 15200 Prague, Czechia

⁶Institute of Applied Geosciences, Graz University of Technology, Rechbauerstraße 12, Graz 8010, Austria

*Corresponding author: bernecker@em.uni-frankfurt.de

Keywords: Δ_{47} , Δ_{48} , carbonate clumped isotopes, acid fractionation factors

Abstract (max. 500)

Due to the lack of direct methods capable of determining the abundance of isotopologues containing multiple heavy isotopes within the crystal lattice, carbonates are typically reacted with phosphoric acid to produce CO₂ analyte for clumped isotope analyses. This reaction is associated with fractionations of both bulk oxygen and clumped isotopes. Accurate knowledge of the effect of cation substitution on the degree of isotopic clumping in the carbonate phase and on acid fractionation factors is crucial for accurate temperature reconstructions based on clumped isotope measurements of extracted CO₂ from various carbonate mineralogies. Previous studies have yielded contradicting results on the effect of carbonate mineralogy on both Δ_{47} acid fractionation factors and the validity of a universal Δ_{47} -T relationship, and, so far, a systematic investigation of mineralogy-specific effects on Δ_{48} is lacking.

In this study, we have analyzed the dual clumped isotope composition of stochastic and non-stochastic calcites, aragonites, dolomites, witherites, and siderites with unprecedented long-term repeatabilities (1SDs) of 8.1 and 28.1 ppm for Δ_{47} and Δ_{48} , respectively. In order to facilitate complete acid digestion of dolomite and siderite in a reasonable timeframe, an acid digestion temperature of 110°C was used for these minerals instead of the 90°C applied to calcite, aragonite and witherite. A set of calcite samples was reacted at both temperatures to determine the calcite-specific difference in acid digestion-related fractionation factors between 90 and 110°C, yielding $\Delta_{47, 110-90^\circ C}^* = -0.0147 \pm 0.002 \%$ and $\Delta_{48, 110-90^\circ C}^* = -0.0148 \pm 0.006 \%$ (2SEs, n=8). After projecting Δ_{47} and Δ_{48} results from stochastic dolomite and siderite to the carbon dioxide equilibrium scale (CDES90) using the calcite-specific $\Delta_{i, 110-90^\circ C}^*$, calcite, aragonite, dolomite, witherite and siderite exhibit statistically indistinguishable $\Delta_{47, CDES90}$ and $\Delta_{48, CDES90}$ values, with weighted averages of

44 0.1850±0.0042 ‰ and 0.1255±0.0130 ‰ (weighted 2SEs, n=15), respectively. In addition,
 45 $\Delta_{47, CDES90}$ and $\Delta_{48, CDES90}$ values of non-stochastic aragonites (n=2), (proto-)dolomites (n=2)
 46 and witherite (n=1) correspond to calcite equilibrium values predicted by their independently
 47 known formation temperatures (Fiebig et al., 2024). Natural dolomites and siderites of
 48 unknown formation temperature are also indistinguishable from the calcite equilibrium line.
 49 Overall, these results imply that calcite, aragonite, dolomite and witherite share
 50 indistinguishable Δ_{47}^* , Δ_{48}^* and $\Delta_{63}-\Delta_{64}-T$ relationships. As a consequence, the calcite-specific
 51 equilibrium $\Delta_{47, CDES90}-\Delta_{48, CDES90}-T$ relationships of Fiebig et al. (2024) can be reliably
 52 applied to aragonite, dolomite, and witherite. More precipitation experiments under
 53 controlled conditions are necessary to clarify with more confidence if these relationships are
 54 also valid for siderite.

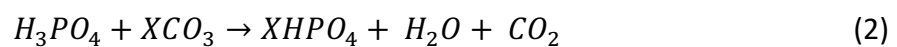
57 1. Introduction

58 Carbonate clumped isotope analysis concerns the determination of the abundances of
 59 carbonate isotopologues in which at least two light isotopes are substituted by their heavy
 60 homologues. The Δ_i metric expresses the extent to which clumped isotopologues are
 61 enriched relative to stochastically driven partitioning of isotopes amongst isotopologues
 62 (Ghosh et al., 2006; Schauble et al., 2006; Wang et al., 2004), see Equation 1, where $R_i = \frac{m/z_i}{m/z_{44}}$
 63 and R_i^* is the stochastically expected isotopologue abundance as determined based on the
 64 bulk isotopic composition (for i in 47, 48 and 49).

$$\Delta_i = \left(\frac{R_i}{R_i^*} - 1 \right) \times 1000 [\text{‰}] \quad (1)$$

65 Departures from stochastic partitioning are due to the slight mass differences between
 66 isotopes and isotopologues, thus influencing molecular vibrational zero-point energies
 67 (Bigeleisen, 1965), making ‘clumped’ arrangements of heavy isotopes thermodynamically
 68 favorable over stochastic arrangements. Because direct determination of clumped CaCO₃
 69 isotopologues from within the crystal lattice is not technically feasible, it is measured on CO₂
 70 released from phosphoric acid digestion of the carbonate (Ghosh et al., 2006).

71 Since the pioneering isotope studies on carbonate minerals (McCrea, 1950; Urey, 1947), it has
 72 been shown many times that acid digestion is associated with oxygen isotope fractionation,
 73 such that the oxygen isotope composition of the evolved CO₂ ($\delta^{18}O_{CO_2}$) is enriched relative
 74 to that of the carbonate ($\delta^{18}O_{XCO_3}$). This occurs because only 2/3 of all oxygen atoms in the
 75 carbonate ion are released as CO₂, whereas 1/3 of the oxygen atoms partition into water; see
 76 Equation 2, where X is a divalent cation, e.g., Ca²⁺, Mg²⁺, Fe²⁺ or Ba²⁺



77 Sharma and Clayton (1965) have already demonstrated differences in oxygen isotope
 78 fractionation factors associated with acid digestion ($^{18}\alpha_{CO_2-XCO_3}$; Equation 3) for different
 79 carbonate minerals

$$^{18}\alpha_{CO_2-XCO_3} = \frac{(\delta^{18}O_{CO_2} + 1000)}{(\delta^{18}O_{XCO_3} + 1000)} \quad (3)$$

80 Follow-up studies have progressively applied more advanced methodologies and empirically
 81 tested a variety of carbonate minerals, thus confirming mineral-specific $^{18}\alpha_{CO_2-XCO_3}$ (e.g.,
 82 Böttcher, 1996; Gilg et al., 2003; Kim & O'Neil, 1997; Rosenbaum & Sheppard, 1986). It has
 83 been shown that the extent of acid fractionation is affected by acid temperature (McCrea,
 84 1950), acid concentration (Wendeborg et al., 2011), reaction time and technique (Swart et al.,
 85 1991), carbonate crystal structure (i.e., rhombohedral calcite group vs. orthorhombic
 86 aragonite group; Gilg et al., 2003; Sharma & Clayton, 1965), different cation substitutions
 87 (Guo et al., 2009), as well as the grain size of reacted carbonate powders (Swart et al., 1991;
 88 Walters et al., 1972).

89 As observed for bulk oxygen isotopes, the clumped isotope compositions of CO₂ (Δ_{47} , Δ_{48} and
 90 Δ_{49}) are likewise offset by acid fractionation factors (i.e., Δ_{47}^* , Δ_{48}^* and Δ_{49}^*) from those of XCO₃
 91 precursor molecules within the crystal lattice (Δ_{63} , Δ_{64} and Δ_{65} , respectively) (e.g., Guo et al.,
 92 2009):

$$\Delta_{47} = \Delta_{63} + \Delta_{47}^* [\text{‰}] \quad (4)$$

$$\Delta_{48} = \Delta_{64} + \Delta_{48}^* [\text{‰}] \quad (5)$$

$$\Delta_{49} = \Delta_{65} + \Delta_{49}^* [\text{‰}] \quad (6)$$

93 Clumped isotope acid fractionation factors Δ_i^* (AFFs), therefore describe the extent to which
 94 bonds between light isotopes are preferentially broken over those of heavy isotopes during
 95 acid digestion of carbonates. The magnitude of these AFFs depends on reaction temperature
 96 (e.g., Guo et al., 2009; Defliese et al., 2015), and possibly on mineralogy (e.g., Guo et al., 2009),
 97 with $\Delta_{i, T1-T2}^*$ representing the difference between temperatures T1 and T2 in °C for a given
 98 mineralogy. The evolved CO₂ gas is enriched in heavy isotopologues, when compared to the
 99 initial CaCO₃ phase (Ghosh et al., 2006). Direct determination of Δ_i^* can be achieved through
 100 analysis of CO₂ derived from phosphoric acid digestion of samples that are characterized by
 101 stochastic distribution of isotopes amongst carbonate isotopologues, i.e., Δ_{63} , Δ_{64} , and Δ_{65} =
 102 0‰ (Schauble et al., 2006; Hill et al., 2014). For the identification of the effects of cation
 103 substitution and crystal structure on Δ_{63} , Δ_{64} and Δ_{65} values, additional analysis of samples
 104 of non-stochastic composition and known formation temperatures is required, since
 105 equilibrium Δ_{63} - Δ_{64} - Δ_{65} values may have mineralogy-dependent temperature sensitivities.
 106 Schauble et al. (2006) and Hill et al. (2014) have calculated equilibrium constants for individual
 107 CO₃²⁻ groups using first-principles lattice dynamics. These predicted that aragonite, calcite,
 108 dolomite and witherite differ in their intrinsic Δ_{63} -T relationships by up to 30 ppm. Theoretical
 109 cluster modeling by Guo et al. (2009) indicated additional cation-dependent differences of
 110 ≤30 ppm in AFFs for aragonite, calcite, witherite and dolomite. Predicted combined
 111 differences make up ≤50 ppm of absolute variation in Δ_{47} -T relationships between carbonate
 112 mineralogies at 25°C acid reaction temperatures (Guo et al., 2009). Considering that Δ_{47}^*
 113 decreases with increasing acid digestion temperature, this value may represent an upper
 114 estimate of the Δ_{47} difference that can be expected.

115 Empirical studies on aragonite and calcite implied that both mineralogies share
116 indistinguishable Δ_{47}^* and Δ_{63} -T relationships (Defliese et al., 2015; Wacker et al., 2013). These
117 findings were confirmed in a more recent study (de Winter et al., 2022) utilizing updated
118 IUPAC parameters (Daëron et al., 2016; Schauer et al., 2016) and carbonate-based
119 standardization (Bernasconi et al., 2021). Discrepant results were reported when calcite was
120 compared to dolomite. Some early investigations revealed dolomite-specific Δ_{47}^* (Müller et
121 al., 2017; Murray et al., 2016), whereas others reported no resolvable differences in Δ_{47}^*
122 and/or Δ_{47} -1/T relationships between dolomite and calcite (Bonifacie et al., 2017; Defliese et
123 al., 2015; Winkelstern et al., 2016). The most recent study by Anderson et al. (2024), who
124 considered IUPAC parameters and carbonate-based standardization, supported the
125 hypothesis that dolomite and calcite share common Δ_{47}^* and Δ_{47} -T relationships.

126 New generations of mass spectrometers have improved Δ_{47} repeatability by a factor of ca. 2-
127 3 compared to the previously described studies. This is due to the improvements in the
128 suppression of secondary electrons which otherwise would lead to a negative bias in mass
129 signals (commonly referred to as pressure baseline, PBL), and the utilization of high-ohmic
130 Faraday cups including a m/z 47.5 half-mass cup for continuous PBL monitoring (Fiebig et al.,
131 2019). Additionally, investigation of Δ_{48} simultaneously to Δ_{47} with long-term repeatabilities
132 approaching theoretical shot-noise limits became possible (Bernecker et al., 2023; Fiebig et
133 al., 2019). Through these so-called “dual clumped” isotope measurements, the effect and
134 relevance of rate-limiting kinetics on the clumped and bulk isotopic compositions of natural
135 carbonates could be identified (Bajnai et al., 2020; Fiebig et al., 2019). Archives characterized
136 by Δ_i values that are not solely controlled by precipitation temperature include warm- and
137 cold-water corals (Davies et al., 2022), brachiopods (Davies et al., 2023), authigenic methane
138 seep carbonates (Staudigel et al., 2024), and eggshell calcite of birds (Tagliavento et al., 2023).
139 With these improvements, even a temperature trend for Δ_{49} has been resolved (Bernecker
140 et al., 2023).

141 Currently, there is no study available that has investigated the effect of cation substitution on
142 the Δ_{48} value of the CO₂ extracted from carbonates. We have analyzed aragonite, calcite,
143 dolomite, siderite and witherite samples, both of known “cold” formation temperature, and
144 re-ordered at $\geq 800^\circ\text{C}$, using the latest high-precision technology (Bernecker et al., 2023) to
145 investigate potential differences in Δ_{47}^* , Δ_{48}^* and Δ_{63} - Δ_{64} -1/T relationships between these
146 carbonate mineralogies. We demonstrate that aragonite, calcite, dolomite, and witherite
147 reacted at temperatures $\geq 90^\circ\text{C}$ share indistinguishable Δ_{47}^* , Δ_{48}^* and Δ_{47} - Δ_{48} -T equilibrium
148 relationships.

149

150 2. Methods

151 2.1 Samples

152 Sample material was crushed using mortar and pestle, sieved using a 200 μm mesh sieve
153 before stored in a 30°C vacuum dry oven and finally weighed out into Ag-capsules to be
154 loaded into the autosampler for dual clumped isotope analysis.

155

156 **2.1.1 Samples heated to temperatures $\geq 800^\circ\text{C}$**

157 Samples of aragonite, calcite, dolomite, siderite and witherite were re-ordered at
 158 temperatures between 800 and 1200°C, through piston cylinder experiments (Section 2.2).
 159 Temperature and pressure were conditioned to match the respective stability fields of these
 160 mineralogies (Table 1). Additionally, we re-analyzed **ETH-1-1100** and **ETH-2-1100**, which were
 161 already utilized for the dual clumped isotope calibration of Fiebig et al. (2021; 2024). These
 162 two samples (former ETH-1 and ETH-2, respectively; Bernasconi et al., 2018; 2021) were
 163 heated to $1,100\pm 10^\circ\text{C}$ at 200 MPa for 24 h. Aragonite sample **Bilin 1(H)**, originally investigated
 164 by Müller et al. (2017), was heated to 850°C at 3.5 GPa for 4 h.

165

166

167 Table 1: Piston cylinder samples and experimental conditions. [†]Unknown heating duration;
 168 temperature remained at 800°C for at least 2 h before sample was quenched.

Acid temp. (°C)	Sample	Temp. (°C)	Duration (h)	Pressure (GPa)	Mineralogy	Reference	
90	Bilin 1(H)	850	4	3.5	Aragonite	Müller et al. (2017)	
90	Arag2-800	800	48	3			
90	Arag1-800	800	72	3			
110	Dolo2_800	800	48	2.5	Dolomite	This study	
110	Dolo1_1200	1,200	53	1.5			
110	Sid_800	800	64	3	Siderite		
90	DIC3-800	800	72	2	Witherite		
90	DIC1-1100	1,100	40	2.3			
90	DIC1-800	800	72	2			
90	ETH-1-800	[†] 800	[†] 48	[†] 1	Calcite		Fiebig et al. (2021, 2024)
90	MERCK-800	800	48	1			
90	ETH-2-800	800	72	1			
90 + 110	ETH-1-1100	1,100	24	0.2			
90	ETH-2-1100	1,100	24	0.2			

169

170

171

172 **2.1.2 Non-heated samples of colder formation temperatures**

173 Dual clumped isotope analyses were carried out on a suite of synthetic and natural carbonate
 174 minerals of both known and unknown formation temperatures (Table 2).

175 Two modern aragonitic bivalve mollusk shells were examined. These were cultured under
 176 controlled temperatures. Sample **AI_006** (*Arctica islandica*) was cultured at NIOZ (Texel, NL)
 177 at 12°C . **RM1** represents the shell of *M modiolus*, which was collected at low tide from a beach

178 in Tentsmuir Forest, southeast Scotland in 2020. The World Ocean Atlas (WOA) lists a mean
 179 annual temperature of 9.7°C and a seasonal amplitude of 6-14°C for the site of collection.
 180 Dolomite calibration samples **Dolomite_350A-9** (dolomitized calcite) and **Dolomite_80-1**
 181 (direct precipitation) of known experimental temperatures (351.4±2 and 80.2±2°C,
 182 respectively) were originally described in detail by Horita (2014) and were later analyzed for
 183 their Δ_{47} -T relationships (Anderson et al., 2024; Bonifacie et al., 2017). **Dolomite_BE**
 184 constitutes a natural low-temperature (25±4°C) dolomite, precipitated in a shallow (<0.5 m),
 185 hypersaline lagoon near Rio de Janeiro (Bonifacie et al., 2017). **IPGP-SRM88-1** and **IPGP-INYO**
 186 are dolomite samples of unknown formation temperature, originating from a batch utilized
 187 as in-house standard at the clumped isotope laboratory at IPGP, the latter of which has been
 188 analyzed for Δ_{47} by Anderson et al. (2024). A suite of dolomite samples originates from a
 189 diagenetically overprinted lacustrine section of the Eger Graben, and is Miocene (Burdigalian)
 190 in age (Rojik, 2004) Dolomitic samples **D-Mio** originate from dolomite-bearing claystone and
 191 were taken at different depths from the ca. 70 m thick (top-eroded) Cypris Formation,
 192 Sokolov sub-basin (core Dp-333 at CGS core repository). Temperature estimates derived from
 193 a mean random vitrinite reflectance of 0.211 ± 0.03 for low thermal maturity organic matter
 194 (Křibek et al., 2017) indicate that the burial temperature experienced by this lithology was
 195 below 60°C.

196 Siderite samples **Sid_D1-Sid_D5** are sub-samples of a 45 cm diameter siderite concretion
 197 retrieved from palustrine deposits within the basal member of the Early Miocene Most
 198 Formation (Bilina Mine, Ústí nad Labem Region, Czech Republic). The alteration aureole
 199 surrounding this concretion in the host rock is represented by **Sid_D6**. **IPGP-Sid1** is a pure
 200 siderite from the La Mûre deposit in France, and has already been investigated for its bulk
 201 isotopic composition (Lebeau et al., 2014).

202 **DIC1** represents a synthetic witherite sample, that has been precipitated by slow addition of
 203 saturated BaCl₂ to an isotopically equilibrated 0.1M NaHCO₃ solution. Both solutions were
 204 produced using the same MilliQ water and thermally equilibrated at 25°C. Addition of BaCl₂
 205 was stopped after 5 % of the DIC pool had been removed through BaCO₃ precipitation. BaCO₃
 206 was removed from the solution by filtration, rinsed twice with MilliQ water, and finally dried
 207 at 25°C.

208
 209
 210
 211
 212

213 Table 2: Non-heated aragonite, dolomite, siderite and witherite samples of un-/controlled formation
 214 temperatures.

Acid reaction temperature	Sample	Temp.	Mineralogy	Reference
		(°C)		
90	DIC1	25.0	Witherite	This study

90 + 110	RM1	9.7	Aragonite	
90	Al_006	12.0		
110	Dolomite_350A-9	351.4	Dolomite	Bonifacie et al. (2017)
110	Dolomite_BE	25.0		
110	Dolomite_80-1	80.2		
110	IPGP-SRM88-1	-		This study
110	IPGP-INYO	-		Anderson et al. (2024)
110	D-Mio-1798_110C	-		This study
110	D-Mio-3010_110C	-		
110	D-Mio-3016_110C	-		
110	D-Mio-3056_110C	-		
110	D-Mio-474_110C	-		
110	D-Mio-5520_110C	-		
110	IPGP-SID1	-	Siderite	Lebeau et al. (2014)
110	Sid_D1	-		This study
110	Sid_D2	-		
110	Sid_D3	-		
110	Sid_D4	-		
110	Sid_D5	-		
110	Sid_D6	-		

215

216 2.2 Piston cylinder experiments

217 Heating experiments on different carbonate materials were carried out in piston cylinders at
218 800-1,200°C for 2-3 days (Table 1) in the Cosmochemistry, Astrophysics and Experimental
219 Geophysics (CAGE) Laboratory at the Institut de Physique du Globe de Paris (IPGP) following
220 the setup and methods outlined by Siebert et al. (2011). The starting sample was placed in a
221 $\frac{3}{4}$ " or $\frac{1}{2}$ " diameter welded platinum capsule and then in a pressure-transmitting medium
222 (here Talc-Pyrex) to ensure good thermal insulation and hydrostatic containment of the
223 samples.

224 The temperature was measured by a W/Re thermocouple located just above the capsule.
225 After having reached the targeted conditions (Table 1), samples were quenched very fast (ca.
226 500°C/s). In all cases, samples were cooled from equilibration temperature to 200°C in less
227 than 3 s, and to room temperature in around 1 min. Uncertainties are less than 50°C for
228 temperature and around 0.1 GPa for pressure.

229 2.3 XRD

230 Powder x-ray diffraction (XRD) analyses were carried out in the Crystallography/Mineralogy
231 Laboratory of Goethe University Frankfurt am Main, Institute of Geosciences (GU) and at
232 IPGP.

233 XRD analyses at GU were performed on a X-PertPro diffractometer equipped with a linear
234 position-sensitive detector from PANalytical (PIXcel3D) and a Johansson monochromator

235 (Ge 111) using Cu K α 1 radiation and fixed divergence slits. Samples were analyzed in the 5-
236 125° range utilizing a step size of 0.0032826° at 549 s integration time per step. The powder
237 was applied on a silicon single-crystal plate.

238 XRD measurements at IPGP were carried out on an Empyrean diffractometer (Malvern-
239 Panalytical), equipped with a copper tube ($k\alpha=1.541874 \text{ \AA}$) and a PIXcel multichannel
240 detector in capillary configuration. A focusing x-ray mirror was placed in the incident beam
241 path. The angular range was varied from 10 to 80°, with a step size of 0.0131° and a counting
242 time of 40 s.

243

244 2.4 Mass spectrometry

245 2.4.1 Experimental setup

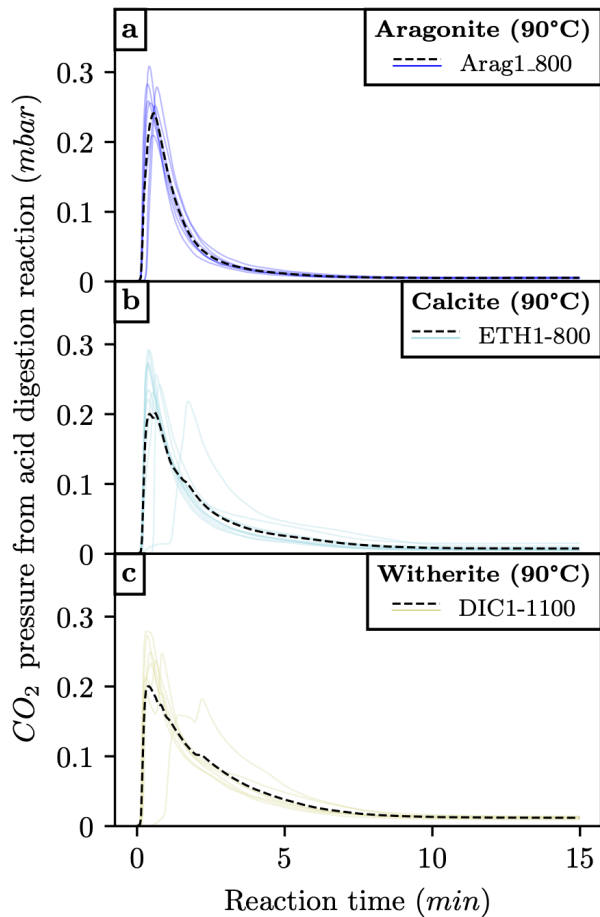
246 Bulk stable and dual clumped isotope analyses were carried out at the Stable Isotope
247 Laboratory at GU following the methodology of Bernecker et al. (2023). Determination of
248 $\delta^{13}\text{C}$, $\delta^{18}\text{O}$, Δ_{47} , Δ_{48} and Δ_{49} is achieved using a Thermo Scientific 253plus gas-source isotope
249 ratio mass spectrometer attached to Hofmann's Auto Line (HAL, Fiebig et al., 2019). Separate
250 analytical sessions were conducted for acid reaction temperatures of 90 and 110°C. Each
251 replicate was measured in at least 13 acquisitions, which were defined by 10 cycles of 20 s
252 integration time each, yielding a minimum total integration time of 2,600 s per replicate.
253 Initial m/z 44 signal intensities for reference and sample gas were adjusted to
254 $16,000 \pm 100 \text{ mV}$ for each acquisition. The CO₂ working gas composition on this setup is
255 $\delta^{13}\text{C}_{VPDB} = -4.21 \text{ ‰}$ and $\delta^{18}\text{O}_{VSMOW} = 25.26 \text{ ‰}$. $\delta^{13}\text{C}_{\text{CO}_2}$ and $\delta^{18}\text{O}_{\text{CO}_2}$ values of unknown
256 samples are reported relative to VSMOW, after normalizing to CO₂ extracted from calcite
257 standards ETH-1 and ETH-2, considering nominal $\delta^{13}\text{C}_{\text{calcite}}$ and $\delta^{18}\text{O}_{\text{calcite}}$ values of
258 Bernasconi et al. (2018) and the $^{18}\alpha_{\text{CO}_2\text{-calcite}}$ at 90°C after Kim et al. (2007). Since the focus
259 of this study is on clumped isotopes, we do not account for differences in $^{18}\alpha_{\text{CO}_2\text{-XCO}_3}$
260 between carbonate mineralogies and reaction temperatures.

261

262 2.4.2 Acid reaction temperature and time needed for quantitative digestion of carbonates in 263 a common acid bath

264 Modern routine setups typically perform reactions at temperatures over 70°C for calcites,
265 with continuous cryogenic removal of CO₂, thereby minimizing the time of CO₂-acid
266 interaction (e.g., Bernasconi et al., 2021). At GU, pressure inside the extraction volume up to
267 the first CO₂ trap is monitored during acid digestion and CO₂ extraction (HAL, Fiebig et al.,
268 2019). For calcitic and aragonitic samples, we generally react $10 \pm 0.2 \text{ mg}$ material per replicate
269 at 90°C acid temperature for 30 min in a magnet bar-stirred common acid bath (CAB).
270 Reaction usually finishes within 10-15 min, when a minimum baseline pressure is
271 asymptotically reached (Figure 1a, b). The same behavior is observed for witherite (Figure 1c)
272 using $19.8 \pm 0.2 \text{ mg}$ of sample material per replicate, in order to produce the same amount of
273 CO₂ analyte.

274

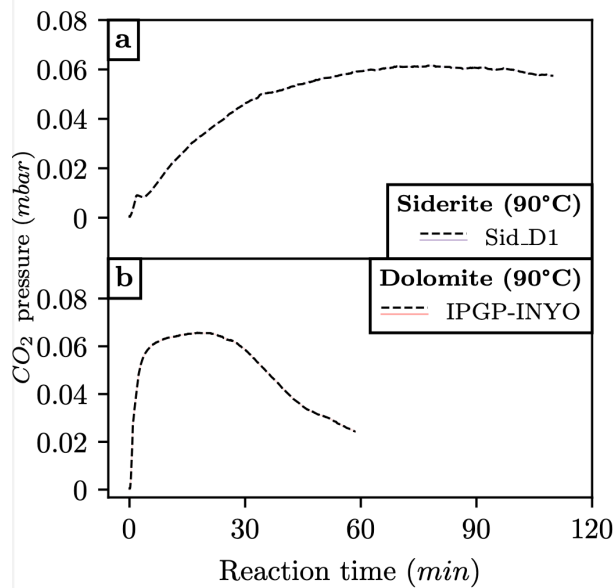


275
276
277
278

Figure 1: CO_2 pressure evolving through acid digestion reactions at 90°C for a) aragonite, b) calcite and c) witherite. Colored thin lines represent individual replicates, the black dashed lines display average CO_2 yields for a given sample.

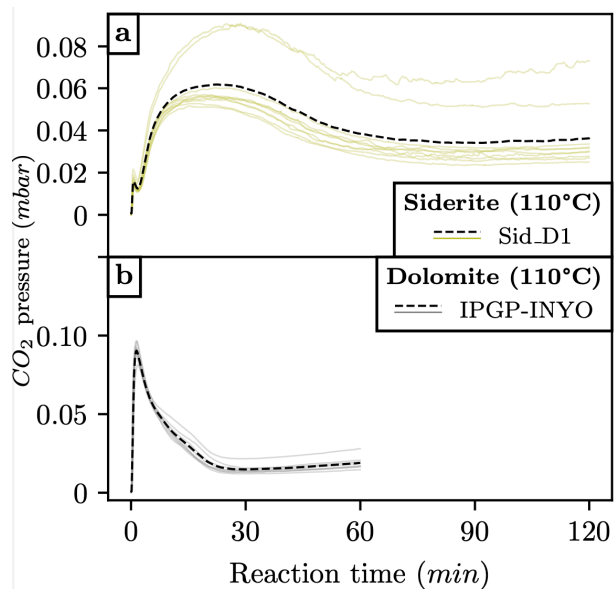
279
280
281
282
283
284
285
286
287
288

Pressure monitoring revealed that a reaction time of 60 min at 90°C is not sufficient to react all dolomite and siderite samples quantitatively. After this period, gas bubbles were not visible anymore, but pressure still evolved non-asymptotically (Figure 2), unlike in calcite, aragonite and witherite reactions (Figure 1). An asymptotic return to minimum pressure values only occurred after increasing the reaction temperature to 110°C , using reaction times of 60 and 120 min for dolomite and siderite, respectively (Figure 3). We monitored the pressure in trap 2 (HAL, Fiebig et al., 2019) and ensured quantitative yields (with mineralogy-dependent weights corresponding to $100\ \mu\text{mol}\ \text{CO}_2$), before analyte CO_2 was entrained at -80°C into the He-carrier gas for GC purification.



289
290 Figure 2: CO₂ pressure evolving through acid digestion reaction at 90°C for a) siderite and b) dolomite.

291



292
293 Figure 3: CO₂ pressure evolving through acid digestion reaction at 110°C for a) siderite and b) dolomite. Colored
294 thin lines represent individual replicates, whereas the black dashed lines display average CO₂ yields for a given
295 sample.

296 Slow, but steadily increasing pressure after the dolomite reactions had finished are due to
297 helium leaking into the reaction chamber. For siderite samples, H₂ formed through oxidation
298 of Fe²⁺ to Fe³⁺ within the acid (Crouzet et al., 2017) is a possible contributor to this elevated
299 final pressure. Because both of these sources of pressure are non-condensable in liquid
300 nitrogen, they are effectively removed during sample gas purification.

301

302

303 2.4.3 Data processing

304 Analytical data was treated following the processing scheme outlined by Bernecker et al.
305 (2023). In short, raw intensity data was corrected for a PBL effect after determination of
306 optimized scaling factors considering sets of gas standards of different bulk isotopic
307 compositions, equilibrated at 25 or 1,000°C (Bernecker et al., 2023; Fiebig et al., 2021). In a
308 next step, baseline-corrected $\delta^{45}\text{-}\delta^{49}$ values were used to perform equilibrated gas-based
309 standardization using nominal theoretical CO₂ equilibrium Δ_{47} (Petersen et al., 2019) and Δ_{48}
310 (Wang et al., 2004; Fiebig et al., 2019) values for CO₂ equilibrated at 25°C and 1000°C and the
311 D47crunch methodology of Daëron (2021), which considers variance minimization of
312 unknowns and anchors. ETH-1, ETH-2, ETH-3 (Bernasconi et al., 2021), ETH-3oxi (Fiebig et al.,
313 2024), Carrara and GU1 (Fiebig et al., 2021) were routinely analyzed along with sample
314 unknowns to account for long-term drifts. Non-bleached replicates of ETH-3 (Bernasconi et
315 al., 2021) were excluded from the variance minimization algorithm of D47crunch (Daëron,
316 2021) as it has been shown that their Δ_{47} and Δ_{48} values were compromised by variable
317 amounts of NO₂ interferent (Fiebig et al., 2024).

318 For the determination of $\Delta_{i, CDES90}$ and $\Delta_{i, CDES110}$ values of unknown samples, D47crunch's
319 *pooled session* processing scheme was applied considering data from all sessions, i.e., not
320 distinguishing between sessions carried out at reaction temperatures of 90 or 110°C. This
321 does not introduce any bias in measured Δ_i values through the variance minimization
322 algorithm inherent to the pooled approach, provided a given carbonate replicate is identified
323 by its sample name *and* reaction temperature. Note that Δ_i values of equilibrated gases are
324 not affected by the acid. Equilibrated gases are only introduced into the gas purification
325 system of HAL after the acid bath (Fiebig et al., 2019).

326 We were not able to adequately standardize and report Δ_{49} data for this study, considering
327 the number of replications per samples in combination with the low signal-to-noise ratio.

328

329 3. Results

330 3.1 XRD

331 Precipitated witherite sample DIC1 and samples heated in piston cylinder experiments were
332 analyzed using X-ray powder diffraction to identify their mineralogy. Diffractograms were
333 compared to those characteristic of the pure mineral phase (RRUFF database, see Lafuente
334 et al., 2015; Supplementary File S3). All diffraction patterns corresponded to those expected
335 for the respective pure minerals.

336

337

338

339

340

341 3.2 Clumped isotopes

342 Δ_{47} and Δ_{48} results for 8 calcitic samples reacted at both 90 and 110°C, are displayed in
 343 Table 3. Bulk ($\delta^{13}C_{VPDB}$, $\delta^{18}O_{VSMOW-CO2}$) and clumped ($\Delta_{47, CDES90}$ and $\Delta_{48, CDES90}$) isotopic
 344 compositions are presented for heated samples in Table 4 and for non-heated samples in
 345 Table 5. The entire dataset, replicate-level $\delta^{45}-\delta^{49}$ values, as well as accompanying results, an
 346 overall sample summary and session-wise standardization parameters are accessible in
 347 Supplementary Tables S1 and S2, respectively.

348 Most heated samples were analyzed with 7-9 replicates, resulting in fully propagated 2SEs of
 349 ca. 7 ppm and 20 ppm for Δ_{47} and Δ_{48} , respectively (Table 4). Hence, we are able to
 350 confidently resolve differences of 10 ppm and 28 ppm in Δ_{47} and Δ_{48} , respectively, which is
 351 comparable to the ≤ 10 ppm, but significantly larger than the ≤ 1 ppm that are theoretically
 352 predicted for Δ_{63} and Δ_{64} , respectively, for aragonite, calcite and dolomite at temperatures
 353 $\geq 800^\circ C$ (Schauble et al., 2006; Hill et al., 2014). Considering our analytical resolution of
 354 10 ppm for Δ_{47} , we cannot resolve any temperature trend in the Δ_{47} data of re-ordered
 355 samples (Table 4). For a given mineralogy and acid digestion temperature, samples heated to
 356 temperatures of 800°C-1,200°C yield Δ_{47} and Δ_{48} values which are within their fully
 357 propagated 2SEs indistinguishable from each other. We are, therefore, confident that a
 358 stochastic distribution has been attained in all our heated samples.

359

360

361 Table 3: Clumped isotope ($\Delta_{47, CDES90}$, $\Delta_{47, CDES110}$, $\Delta_{48, CDES90}$ and $\Delta_{48, CDES110}$) values of samples reacted at 90
 362 and 110°C, respectively. $\Delta_{i, 110-90^\circ C}^*$ corresponds to the difference between $\Delta_{i, CDES90}$ and $\Delta_{i, CDES110}$ values, 2SEs
 363 were determined through Gaussian error propagation of individual 2SEs for CDES90 and CDES110
 364 (Supplementary Table S2).

Sample	N 90°C	N 110°C	$\Delta_{47, CDES90}$ (‰)	$\Delta_{47, CDES110}$ (‰)	$\Delta_{47, 110-90^\circ C}^*$ (‰)	2SE (‰)	$\Delta_{48, CDES90}$ (‰)	$\Delta_{48, CDES110}$ (‰)	$\Delta_{48, 110-90^\circ C}^*$ (‰)	2SE (‰)
Carrara	177	13	0.310	0.294	-0.0155	0.006	0.143	0.126	-0.0174	0.018
DHC2-8	23	7	0.570	0.557	-0.0133	0.008	0.233	0.224	-0.0087	0.026
ETH-1	637	26	0.207	0.194	-0.0126	0.005	0.127	0.122	-0.0050	0.014
ETH-1-1100	11	8	0.182	0.168	-0.0144	0.009	0.116	0.097	-0.0186	0.028
ETH-2	621	25	0.209	0.197	-0.0129	0.004	0.129	0.112	-0.0174	0.013
GU1	163	9	0.225	0.210	-0.0153	0.006	-0.399	-0.427	-0.0267	0.033
SA05	8	8	0.571	0.556	-0.0148	0.009	0.247	0.227	-0.0196	0.030
SA31	11	8	0.588	0.569	-0.0190	0.009	0.247	0.242	-0.0054	0.028
weighted average ($\pm 2SE$)					-0.0147	0.002			-0.0148	0.006

365

366 Table 4: $\delta^{13}C_{VPDB}$, $\delta^{18}O_{VSMOW-CO2}$, $\Delta_{47, CDES90}$ and $\Delta_{48, CDES90}$ values of aragonite, calcite, dolomite, siderite
367 and witherite samples heated in piston cylinder experiments. *Values projected using mean $\Delta_{47, 110-90^\circ C}^*$ and
368 $\Delta_{48, 110-90^\circ C}^*$ values of -0.0147 ± 0.002 ‰ and -0.0148 ± 0.006 ‰, respectively. †Gaussian error propagation of
369 $\Delta_{i, 110-90^\circ C}^*$ 2SE of means (Table 3) and fully error propagated 2SE for Δ_i (Daëron, 2021). #Sample re-ordered at
370 $850^\circ C$.

Sample	N	$\delta^{13}C_{VPDB}$ (‰)	$\delta^{18}O_{VSMOW-CO2}$ (‰)	$\Delta_{47, CDES90}$ (‰)	2SE (‰)	$\Delta_{48, CDES90}$ (‰)	2SE (‰)
<i>Aragonite</i>							
Arag1-800_72h	9	1.87	37.04	0.1877	0.0062	0.1202	0.0198
Arag2-800_48h	10	8.44	31.08	0.1819	0.0059	0.1126	0.0185
Bilin-1H#	9	3.09	31.01	0.1842	0.0061	0.1359	0.0189
<i>Calcite</i>							
ETH-1-1100	11	1.93	36.88	0.1824	0.0057	0.1157	0.0178
ETH-1-1100_110C	8	1.94	36.92	*0.1827	†0.0073	*0.1119	†0.0225
ETH-2-1100	19	-10.13	20.00	0.1826	0.0042	0.1218	0.0136
ETH1-800	10	1.93	36.96	0.1856	0.0059	0.1174	0.0188
ETH2-800_72h	10	-10.2	19.94	0.1863	0.0057	0.1358	0.0185
MERCK-800_48h	9	-42.1	23.07	0.1886	0.0064	0.1261	0.0193
<i>Dolomite</i>							
Dolo1_1200_110C	8	-0.66	32.75	*0.1799	†0.0071	*0.1405	†0.0221
Dolo2_800_110C	8	-0.47	33.18	*0.1770	†0.0072	*0.1406	†0.0221
<i>Siderite</i>							
Sid_800_64h_110C	8	-12.33	23.79	*0.1738	†0.0070	*0.1274	†0.0220
<i>Witherite</i>							
DIC1-1100_40h	7	-5.97	25.49	0.1808	0.0068	0.1096	0.0217
DIC1-800_72h	7	-6.00	25.12	0.1853	0.0068	0.1366	0.0217
DIC3-800_72h	9	-5.18	30.48	0.1847	0.0060	0.1101	0.0194

371

372 Table 5: $\delta^{13}C_{VPDB}$, $\delta^{18}O_{VSMOW-CO2}$, $\Delta_{47, CDES90}$ and $\Delta_{48, CDES90}$ results for aragonite, dolomite, witherite and
373 siderite samples of un-/controlled lower formation temperature. *Values projected using mean $\Delta_{47, 110-90^\circ C}^*$ and
374 $\Delta_{48, 110-90^\circ C}^*$ of -0.0147 ± 0.002 ‰ and -0.0148 ± 0.006 ‰, respectively. [¶]Gaussian error propagation of Δ_i^* , $110-90^\circ C$
375 2SE of means (Table 3) and fully error propagated 2SE for Δ_i (Daëron, 2021). [†]Considered proto-dolomite.

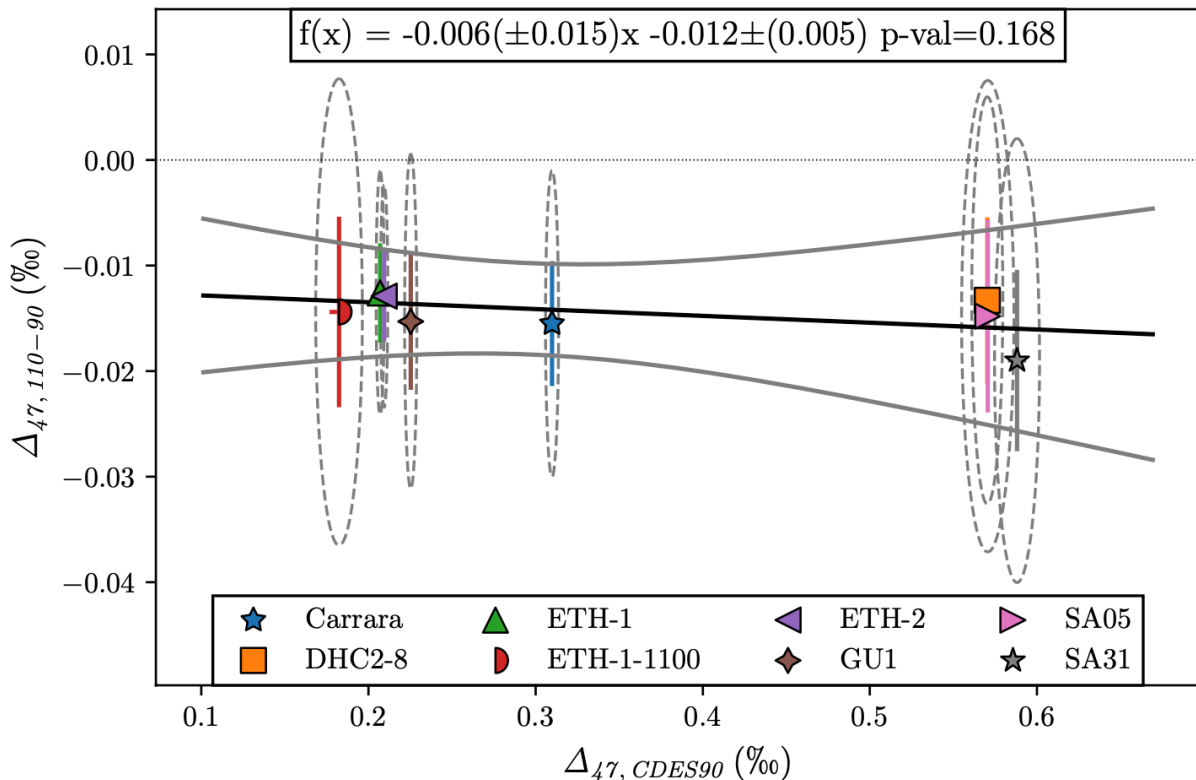
Sample	N	$\delta^{13}C_{VPDB}$ (‰)	$\delta^{18}O_{VSMOW-CO2}$ (‰)	$\Delta_{47, CDES90}$ (‰)	2SE (‰)	$\Delta_{48, CDES90}$ (‰)	2SE (‰)
<i>Aragonite</i>							
AI_006	7	0.05	41.79	0.632	0.007	0.271	0.023
RM1	9	1.49	41.12	0.646	0.007	0.255	0.022
RM1 (110°C)	9	1.61	41.16	*0.634	[¶] 0.007	*0.250	[¶] 0.021
TS2	8	-7.42	36.69	0.597	0.006	0.240	0.021
<i>Dolomite</i>							
D-Mio-1798	6	2.40	34.80	*0.529	[¶] 0.009	*0.207	[¶] 0.027
D-Mio-3010	6	4.24	33.25	*0.526	[¶] 0.009	*0.190	[¶] 0.027
D-Mio-3016	6	4.32	33.43	*0.521	[¶] 0.009	*0.223	[¶] 0.028
D-Mio-3056	6	5.16	34.12	*0.540	[¶] 0.009	*0.247	[¶] 0.028
D-Mio-474	6	3.40	33.19	*0.540	[¶] 0.009	*0.219	[¶] 0.027
D-Mio-5520	6	8.14	36.68	*0.552	[¶] 0.010	*0.207	[¶] 0.027
Dolomite_350A-9	7	-55.72	7.06	*0.246	[¶] 0.008	*0.148	[¶] 0.024
Dolomite_80-1 [†]	8	-6.74	23.95	*0.468	[¶] 0.007	*0.331	[¶] 0.023
Dolomite_BE	9	-10.02	44.07	*0.593	[¶] 0.007	*0.252	[¶] 0.022
IPGP-SRM88-1	8	2.20	32.87	*0.502	[¶] 0.007	*0.206	[¶] 0.022
IPGP-INYO	9	-0.61	32.90	*0.236	[¶] 0.007	*0.136	[¶] 0.021
<i>Siderite</i>							
IPGP-SID1	8	-12.20	23.86	*0.307	[¶] 0.007	*0.165	[¶] 0.022
Sid_D1	10	14.11	34.37	*0.559	[¶] 0.007	*0.238	[¶] 0.020
Sid_D2	10	17.23	36.54	*0.590	[¶] 0.007	*0.244	[¶] 0.021
Sid_D3	10	18.58	37.21	*0.588	[¶] 0.007	*0.251	[¶] 0.021
Sid_D4	9	18.51	37.12	*0.592	[¶] 0.007	*0.244	[¶] 0.021
Sid_D5	9	15.42	35.31	*0.568	[¶] 0.007	*0.238	[¶] 0.021
Sid_D6	10	-10.53	31.76	*0.511	[¶] 0.006	*0.219	[¶] 0.020
<i>Witherite</i>							
DIC1	6	-5.86	26.18	0.590	0.007	0.260	0.023

376

377 3.3 Determination of the difference in acid fractionation factors between 90 and
 378 110°C reactions

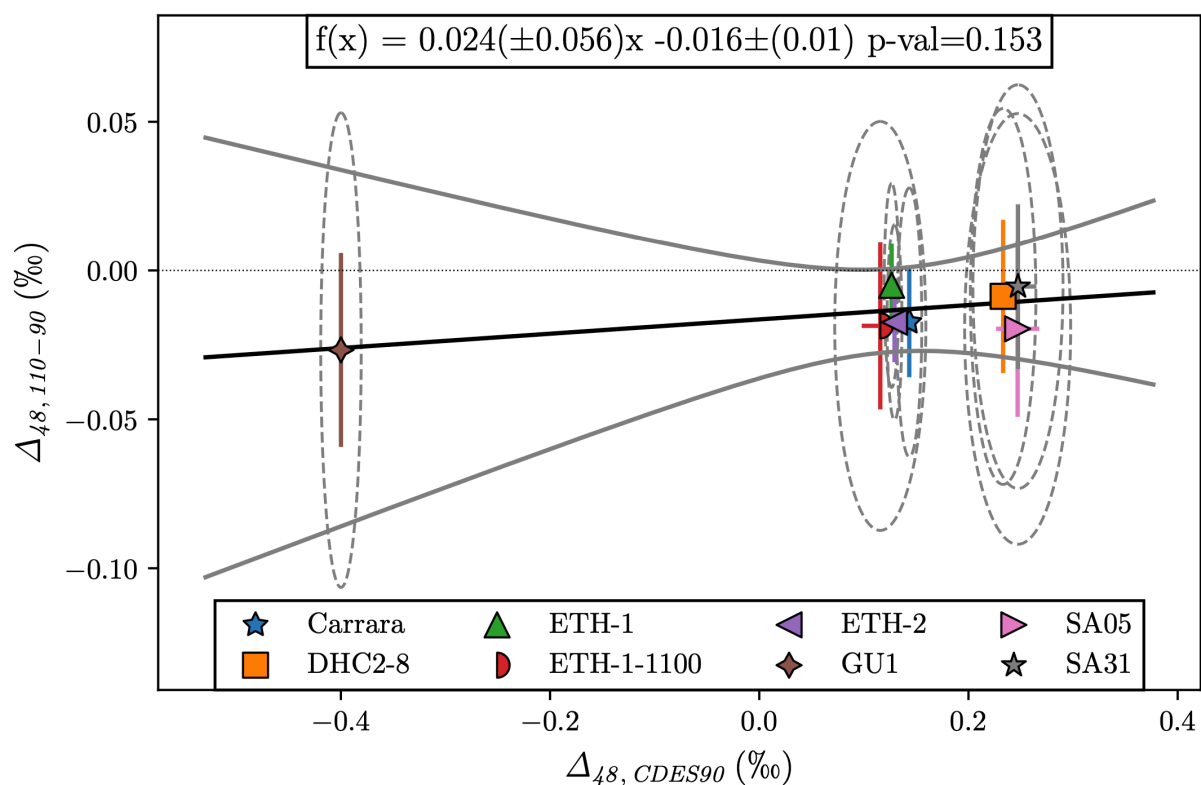
379 In order to quantify the effect of acid digestion temperature on measured Δ_{47} and Δ_{48} values,
 380 we analyzed a suite of calcites at both 90 and 110°C. This enables determining differences in
 381 $\Delta_{i, CDES110} - \Delta_{i, CDES90}$ values, expressed as $\Delta_{i, 110-90}^*$. Guo et al. (2009) predicted a weak
 382 temperature dependence of 0.035‰ in $\Delta_{47, 25^\circ C}^*$ for every 1‰ increase in Δ_{63} , due to the
 383 circumstance that ^{17}O -bearing isotopologues contribute slightly, but in different proportions
 384 to overall masses 63 and 47. On the contrary, the contribution of ^{17}O -bearing isotopologues
 385 to overall masses 64 and 48 is negligibly small, such that Δ_{64} is not expected to affect Δ_{48}^*
 386 significantly at any digestion temperature. In any case, compositional effects occurring at acid
 387 digestion temperatures of 90°C and 110°C should cancel each other out if the difference in
 388 acid fractionation factors $\Delta_{i, 110-90}^*$ is addressed. As expected, no significant slope is found
 389 for correlations between $\Delta_{47, 110-90}^*$ and $\Delta_{47, CDES90}$ (as a measure of Δ_{63}) and between
 390 $\Delta_{48, 110-90}^*$ and $\Delta_{48, CDES90}$ (as a measure of Δ_{64}) (see Figures 4 and 5). Throughout the
 391 following, we use average $\Delta_{47, 110-90}^*$ and $\Delta_{48, 110-90}^*$ values of -0.0147 ‰ and -0.0148 ‰,
 392 respectively, to project CDES110 data to the CDES90. We further assume that these calcite-
 393 specific $\Delta_{i, 110-90}^*$ are also valid for dolomite and siderite.

394



395

396 Figure 4: Differences between $\Delta_{47, CDES90}$ and $\Delta_{47, CDES110}$ (i.e., $\Delta_{47, 110-90}^*$) as a function of $\Delta_{47, CDES90}$ for
 397 several calcite samples. No significant correlation is observed, as demonstrated through p-value >0.05 when
 398 using OGLS regression (Daëron & Vermeesch, 2024).



399
 400 Figure 5: Differences between $\Delta_{48, CDES90}$ and $\Delta_{48, CDES110}$ (i.e., $\Delta_{48, 110-90}^*$) as a function of $\Delta_{47, CDES90}$ for
 401 several calcite samples. No significant correlation is observed, as demonstrated through p-value >0.05 when
 402 using OGLS regression (Daëron & Vermeesch, 2024).

403 4. Discussion

404 4.1 Acid fractionation factors derived from samples heated to stochastic composition

405 According to the theoretical model of Guo et al. (2009), differences of up to 30 ppm in Δ_{47}^* for
 406 aragonite, calcite, witherite and dolomite were predicted. Δ_{47}^* has been determined
 407 experimentally by Guo et al. (2009), who melted three calcitic samples, reacted these directly
 408 at 25°C and obtained an average Δ_{47}^* of 0.232 ± 0.015 ‰ (1SD) on the internal Caltech scale.
 409 Later, following the introduction of the absolute reference frame (ARF) by Dennis et al.,
 410 (2011), Passey & Henkes (2012) heated calcite to a temperature of 800°C and reacted this
 411 sample at 90°C. Their resulting $\Delta_{47, CDES90}^*$ value of 0.213 ‰ corresponded to a $\Delta_{47, CDES25}^*$
 412 value of 0.294 ‰, considering the $\Delta_{47, 90-25}^*$ of -0.081 ‰ of Passey et al. (2010). This
 413 $\Delta_{47, CDES25}^*$ value agreed with the $\Delta_{47, CDES25}^*$ value of 0.280 ± 0.016 ‰ (error represents
 414 replicate-based 1SD) reported by Tripathi et al. (2015), who reprocessed the data of Guo et al.
 415 (2009) using heated gases and NBS 19 as anchors for ARF projection (Dennis et al., 2011). For
 416 a melted witherite sample, Tripathi et al. (2015) reported a $\Delta_{47, CDES90}^*$ value of 0.163 ± 0.006 ‰
 417 (error represents replicate-based 1SD), which was projected into the CDES25 using
 418 $\Delta_{47, 90-25}^*$ of -0.092 ‰ (Henkes et al., 2013), finally yielding a $\Delta_{47, CDES25}^*$ value of
 419 0.255 ± 0.006 ‰ (1SD), i.e., significantly lower than the one reprocessed for calcite. A more
 420 comprehensive study of Müller et al. (2017) investigated the Δ_{47}^* values of aragonite, calcite
 421 and dolomite which were heated to temperatures $\geq 850^\circ\text{C}$. They reacted samples both at 70°C

422 using the Kiel IV setup and offline in McCrea type reaction vessels at 100°C. The CO₂ released
423 at 70°C was introduced into the mass spectrometer using the micro volume mode of the
424 Kiel IV, whereas the dual inlet was used for the CO₂ extracted at 100°C. They obtained
425 significantly distinct AFFs for 70°C reactions of aragonite ($\Delta_{47, CDES70}^* = 0.172 \pm 0.003$), calcite
426 ($\Delta_{47, CDES70}^* = 0.197 \pm 0.002$) and dolomite ($\Delta_{47, CDES70}^* = 0.226 \pm 0.002$, errors representing non-
427 propagated, replicate-based 1SE). Their study, therefore, confirmed that calcite and dolomite
428 may exhibit different Δ_{47}^* -T_{acid} relationships, as originally postulated by Murray et al. (2016).
429 Bonifacie et al. (2017) indirectly estimated that the AFF at 90°C for dolomite was $\Delta_{47, CDES90}^*$
430 = 0.176 ‰, by comparing their $\Delta_{47, CDES90}$ -T calibration regression line based on dolomites
431 covering a large range of formation temperatures (between 25 and 350°C) with the
432 theoretically determined Δ_{63} -T relationship for dolomite (Schauble et al., 2006). As expressed
433 by these authors, this value was slightly lower than the $\Delta_{47, CDES90}^*$ value of 0.198 ± 0.008 ‰
434 obtained from the intercept of the $\Delta_{47, CDES25}$ -T relationship by Passey & Henkes (2012)
435 corrected for their experimentally determined $\Delta_{47, 90-25}^*$, but matched the internal Caltech
436 scale $\Delta_{47, 25}^*$ value of melted calcites from Guo et al. (2009) after projecting this value into
437 the CDES90 using the Caltech-specific tertiary transfer function of Dennis et al. (2011). Based
438 on this observation and their additional finding that $\Delta_{47, CDES90}$ values obtained on calcite and
439 dolomite were comparable, Bonifacie et al (2017) proposed that calcite and dolomite exhibit
440 not only similar $\Delta_{47, CDES90}^*$, but also comparable $\Delta_{47, CDES90}$ -T relationships.

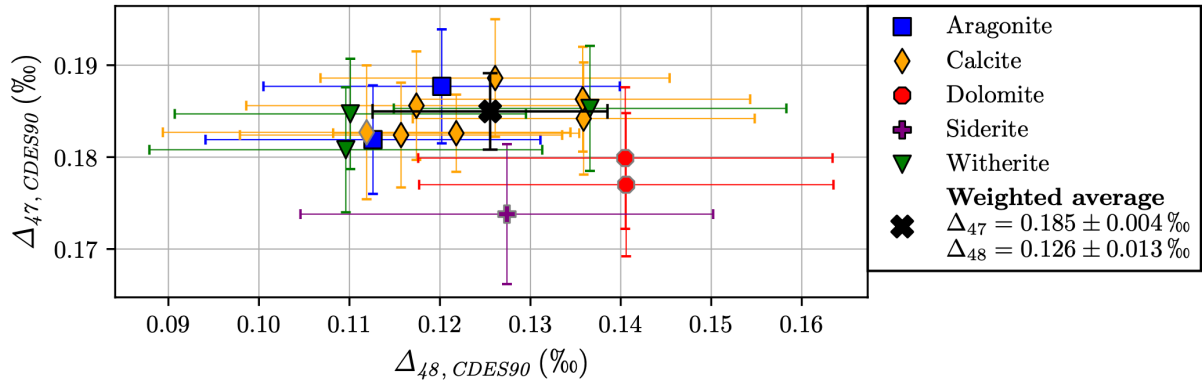
441 All analytical measurements for the aforementioned studies were produced using the first
442 generation of gas source mass spectrometers. Accuracy and precision of corresponding
443 measurements were likely affected by non-optimal correction for the negative PBL effect
444 (Fiebig et al., 2016). In addition, non-unique temperature dependencies of AFFs were
445 considered for the comparison of Δ_{47} values obtained at different reaction temperatures
446 (Petersen et al., 2019). Ultimately, non-optimal ¹⁷O correction parameters (Daëron et al.,
447 2016; Petersen et al., 2019; Schauer et al., 2016) were used in some of these studies, and full
448 error propagation (Daëron, 2021) was not considered. Recently, Fiebig et al. (2021) reacted
449 two calcites heated at 1,100°C in a CAB and obtained $\Delta_{47, CDES90}^*$ values of 0.179 ± 0.006 ‰
450 and 0.184 ± 0.006 ‰ (fully error propagated 2SE). Anderson et al. (2024) reacted dolomites
451 which were re-ordered at 1,100-1,200°C, at an acid digestion temperature of 70°C. They
452 projected mass spectrometric raw data to a reaction temperature of 90°C using calcite
453 anchors ETH-1, ETH-2, ETH-3, ETH-4 and IAEA-C2 (Bernasconi et al., 2021), finally obtaining
454 $\Delta_{47, I-CDES}^*$ values ranging from 0.180 to 0.184 ‰ (Anderson et al., 2024). Note that I-CDES
455 values should perfectly align with CDES90 values since the former scale has been anchored
456 relative to the latter. Furthermore, these values agreed perfectly with the calcite-specific
457 $\Delta_{47, CDES90}^*$ values of Fiebig et al. (2021), suggesting that calcite and dolomite have
458 indistinguishable Δ_{47}^* for a given acid reaction temperature in the range of 70-90°C. Latest I-
459 CDES results of Kong et al. (2023) implied that AFFs for witherite and calcite are identical as
460 well. These authors reacted witherite reordered at 600°C at an acid digestion temperature of
461 90°C, obtaining a $\Delta_{47, I-CDES}$ value of 0.213 ± 0.021 ‰. This value is indistinguishable from the

462 $\Delta_{47,I-CDES}$ values of 0.2052 ± 0.0016 ‰ and 0.2085 ± 0.0015 ‰ assigned to ETH-1 and ETH-2,
463 respectively, which represent calcites that were also equilibrated at 600°C (Bernasconi et al.,
464 2021).

465 To make our clumped isotope data generated at the two distinct temperatures of 110°C and
466 90°C comparable, we projected all CDES110 data into the CDES90 using our calcite-specific
467 $\Delta_{47,110-90^\circ C}^*$ and $\Delta_{48,110-90^\circ C}^*$ values (Table 4, Section 3.3, Figure 6). Doing so, we inherently
468 assume that calcite-specific $\Delta_{47,110-90^\circ C}^*$ and $\Delta_{48,110-90^\circ C}^*$ are also valid for all other
469 investigated mineralogies. Considering the limited sample sizes (i.e., number of replicates) of
470 each individual group of stochastic samples (n between 1 and 6 across five groups), classic
471 parametric tests, such as ANOVA and t-tests are not applicable to identify significant
472 differences in $\Delta_{47,CDES90}^*$ and $\Delta_{48,CDES90}^*$ values between groups. Instead, we employed non-
473 parametric tests which do not rely on distributional assumptions and are more robust in this
474 context (Zimmerman, 2000). We used the Kruskal-Wallis H-test for overall group
475 comparisons, as it can handle groups of different sizes and does not assume normality
476 (Kruskal & Wallis, 1952). Additionally, for pairwise comparisons, we utilized Mann-Whitney U
477 tests, which are suitable for small, unequal sample sizes (Mann & Whitney, 1947). Both the
478 Kruskal-Wallis H-test ($H=7.17$, $p=0.127$ and $H=5.81$, $p=0.214$, respectively) and the pairwise
479 Mann-Whitney U tests (all corr. $p\geq 0.71$) revealed no significant difference in $\Delta_{47,CDES90}^*$ and
480 $\Delta_{48,CDES90}^*$ values between stochastic calcite, aragonite, dolomite, witherite and siderite. Only
481 one thermally reset siderite sample was measured, therefore, we cannot guarantee that its
482 corresponding $\Delta_{47,CDES90}^*$ and $\Delta_{48,CDES90}^*$ values are perfectly representative. However,
483 Holme et al. (2023) reacted siderite and calcite at 90°C using a CAB. Three replicates of a
484 siderite equilibrated at 625°C yielded a mean $\Delta_{47,CDES90}$ value of 0.206 ± 0.006 ‰ (1 SE). This
485 value is in excellent agreement with $\Delta_{47,CDES90}$ values obtained for InterCarb calcite anchors
486 ETH-1 (0.2052 ± 0.0016 ‰) and ETH-2 (0.2085 ± 0.0015 ‰; 1SEs), both of which were heated
487 to 600°C (Bernasconi et al. 2021). Their results, therefore, seem to confirm that calcite and
488 siderite have indistinguishable $\Delta_{47,CDES90}^*$.

489 We conclude that there is no indication for significant differences in Δ_{47}^* and Δ_{48}^* values
490 between calcite, aragonite, dolomite, witherite and siderite at a given temperature in the
491 range 90-110°C. The overall error-weighted average $\Delta_{47,CDES90}^*$ value is 0.1850 ± 0.0042 ‰ and
492 the $\Delta_{48,CDES90}^*$ value is 0.1255 ± 0.0130 ‰, both in excellent agreement with recently
493 published estimations of calibration intercepts of 0.1848 ‰ and 0.1214 ‰ obtained for
494 calcite (Fiebig et al., 2024).

495

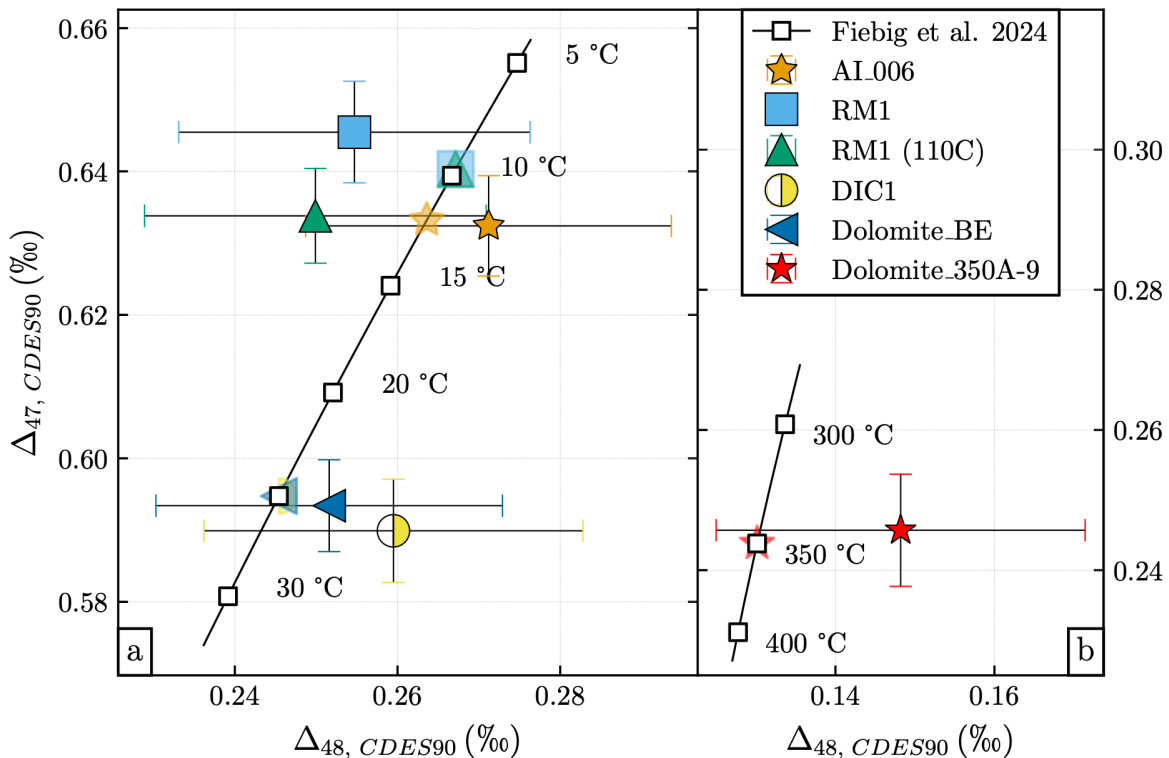


496
497
498
499
500

Figure 6: Dual clumped isotope ($\Delta_{47, CDES90}$ and $\Delta_{48, CDES90}$) results ($\pm 2SE$) for investigated stochastic samples of different mineralogies. CDES110 data (grey outlined markers) was projected into the CDES90 using calcite-derived $\Delta_{47, 110-90^\circ C}^*$ and $\Delta_{48, 110-90^\circ C}^*$ values of -0.0147 and -0.0148 ‰, respectively (Table 3). See text for further information.

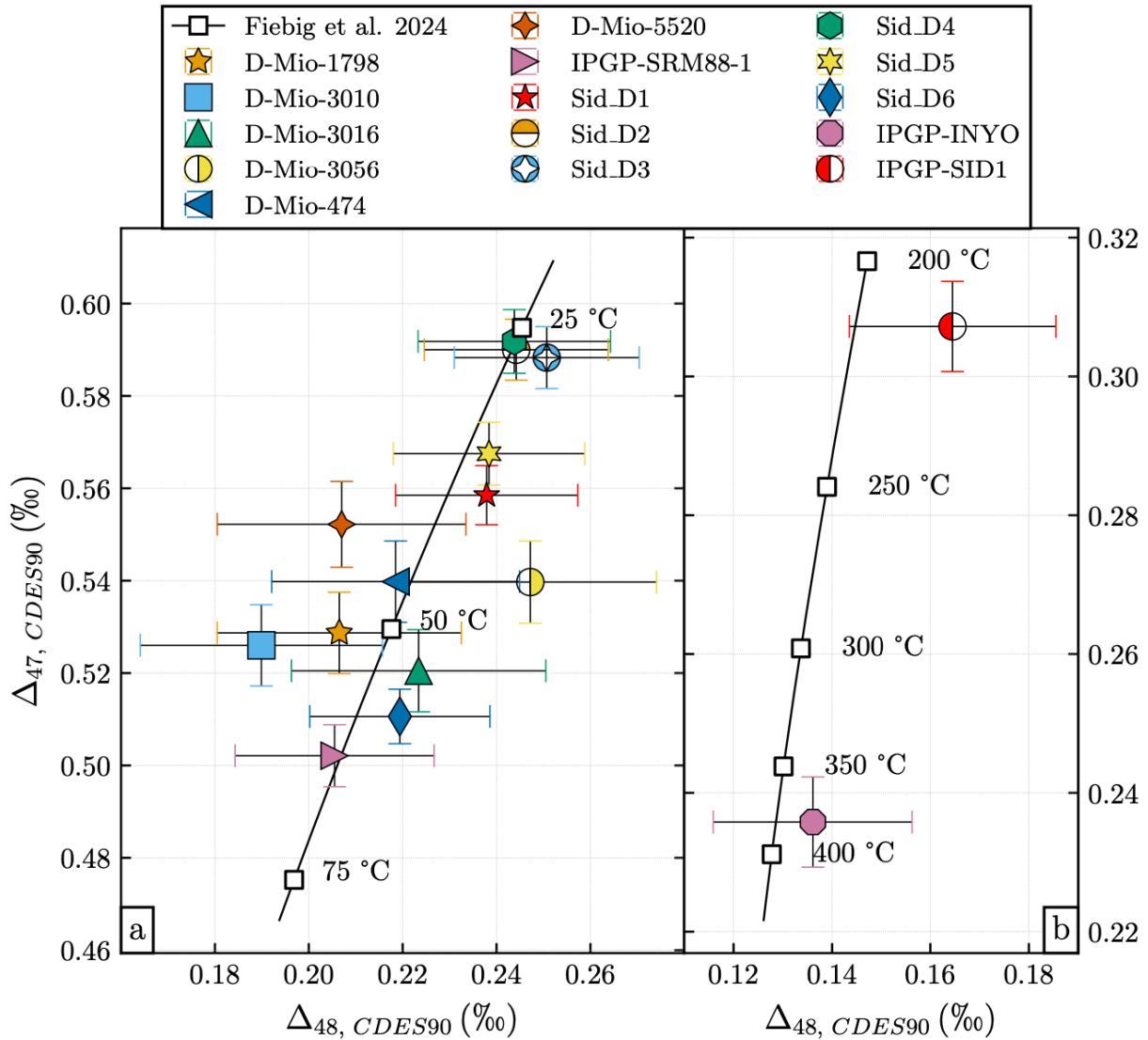
501 4.2 Non-stochastic samples of lower formation temperatures

502 The $\Delta_{47, CDES90}$ and $\Delta_{48, CDES90}$ compositions of non-stochastic samples formed at known and
503 unknown temperatures are shown relative to the calcite equilibrium line (Fiebig et al., 2024)
504 in Figures 7 and 8, respectively. This information, paired with our observations on acid
505 fractionation factors (Section 4.1), can resolve if there is any significant difference in $\Delta_{63}-\Delta_{64}-$
506 T relationships between these minerals.



507
508
509
510
511
512
513

Figure 7: Dual clumped isotope composition ($\Delta_{47, CDES90}$ and $\Delta_{48, CDES90}$) of non-stochastic samples of known lower formation temperatures, displayed relative to the calcite-specific temperature equilibrium relationship (Fiebig et al., 2024). Aragonite sample RM1 (110C) and dolomite samples have been acid digested at $110^\circ C$ and projected into the CDES90 using calcite-derived $\Delta_{47, 110-90^\circ C}^*$ and $\Delta_{48, 110-90^\circ C}^*$ values of -0.0147 ‰ and -0.0148 ‰, respectively (Table 3). Transparent markers on the $\Delta_{47}-\Delta_{48}$ temperature equilibrium line indicate known formation temperatures.



514

515 Figure 8: Dual clumped isotope composition ($\Delta_{47, CDES90}$ and $\Delta_{48, CDES90}$) of non-stochastic samples of unknown
516 lower formation temperatures, displayed relative to the calcite-specific temperature equilibrium relationship
517 (Fiebig et al., 2024). Samples have been acid digested at 110°C and projected into the CDES90 using calcite-
518 derived $\Delta_{47, 110-90^\circ C}^*$ and $\Delta_{48, 110-90^\circ C}^*$ values of -0.0147 ‰ and -0.0148 ‰, respectively (Table 3).

519 4.2.1 Aragonite

520 Early studies on aragonite assumed that the temperature dependences of aragonite- and
521 calcite- Δ_{47} are indistinguishable, thus applying calcite-based calibrations to determine
522 aragonite formation temperature (e.g., Came et al., 2007). Validity of this assumption was
523 confirmed in numerous independent investigations. Tripathi et al. (2010), presenting a Δ_{47} -T
524 calibration on aragonitic and calcitic foraminifera and coccoliths, and Henkes et al. (2013),
525 providing a Δ_{47} -T calibration largely based on aragonitic and calcitic mollusks, did not resolve
526 any significant differences between aragonite and calcite. The first pure synthetic aragonite
527 Δ_{47} -T calibration (Defliese et al., 2015) was indistinguishable from a calcite calibration
528 produced by the same authors, and also from the calcite calibration of Wacker et al. (2014).
529 Kele et al. (2015) reacted aragonite and calcite at 70°C using the Kiel IV analytical setup and
530 showed that both have very similar Δ_{47} -T relationships. Kelson et al. (2017) precipitated

531 calcite and aragonite samples at identical temperatures, reacted at both 25°C and 90°C and
532 likewise found indistinguishable Δ_{47} -T relationships. In a recent, comprehensive study (70°C
533 acid digestion using a Kiel IV, ETH anchor standardization to I-CDES), biogenic (1-18°C) and
534 abiogenic (1-850°C) aragonite samples of controlled formation temperature were analyzed
535 (de Winter et al., 2022). No significant offsets were displayed relative to the unified calibration
536 of Anderson et al. (2021) which is largely based on calcite. So far, studies applying dual
537 clumped isotopes to aragonite have directly applied calcite-specific calibrations to identify
538 kinetic biases and/or infer carbonate formation temperatures (Arndt et al., 2025; Bajnai et
539 al., 2020; Davies et al., 2022; Fiebig et al., 2021; Kniest et al., 2024; Lu et al., 2024; Parvez et
540 al., 2023; Staudigel et al., 2024).

541 Our $\Delta_{47, CDES90}$ and $\Delta_{48, CDES90}$ values for biogenic aragonite samples **AI_006** and **RM1** plot
542 indistinguishably from calcite equilibrium (Figure 7). $\Delta_{47, CDES90}$ -derived temperatures of
543 $12.3^{+2.3}_{-2.3}$ °C (**AI_006**) and $8.1^{+2.3}_{-2.3}$ °C (**RM1**) agree within $\pm 2SEs$ with their formation
544 temperatures of 12.0°C and $9.7^{+4.3}_{-3.7}$ °C, respectively. Sample **RM1** was additionally reacted at
545 110°C (**RM1 (110C)**). Applying calcite-derived $\Delta_{47, 110-90}^*$ and $\Delta_{48, 110-90}^*$ of -0.0147 ‰ and
546 -0.0148 ‰, respectively, to its measured $\Delta_{i, CDES110}$ values finally yields $\Delta_{i, CDES90}$ values
547 which are within 2SEs indistinguishable from those obtained on **RM1**. The $\Delta_{47, CDES90}$ -derived
548 temperature of $11.8^{+2.2}_{-2.1}$ °C is again consistent with the known formation temperature
549 (Figure 7, Table 5).

550 Our high-precision results, therefore, confirm previous evidence that aragonite and calcite
551 follow a single Δ_{47} -T equilibrium relationship. Differences in Δ_{48} are below analytical
552 resolution as well. Considering these indistinguishable AFFs between calcite and aragonite
553 (Section 4.1), we propose that samples of aragonite follow the same Δ_{63} -T and Δ_{64} -T
554 relationships as calcite. Conclusively, the equilibrium Δ_{47} - Δ_{48} -T calibrations of Fiebig et al.
555 (2021; 2024) and Swart et al. (2021), which are indistinguishable from each other within
556 errors, can also be applied to aragonite.

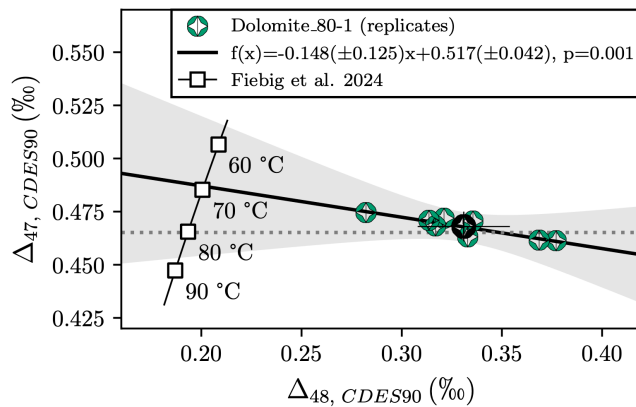
557

558 4.2.2 Dolomite

559 Winkelstern et al. (2016) reacted natural and synthetic dolomites of known formation
560 temperatures (20-250°C) at an acid digestion temperature of 75°C. In the low temperature
561 range, their $\Delta_{47, CDES25}$ -T calibration was indistinguishable from those of Defliese et al. (2015)
562 for calcite and aragonite precipitated at 5-70°C. A single Δ_{47} -T relationship for calcite and
563 dolomite was also proposed by Bonifacie et al. (2017), who reacted at 90°C natural and
564 synthetic samples of controlled formation temperatures (25-350°C). Conversely, differences
565 between calcite and dolomite were reported by Müller et al. (2019). They reacted dolomites
566 of controlled formation temperatures at 70°C and compared the dolomite $\Delta_{47, CDES70}$ -T
567 relationship to the calcite/aragonite $\Delta_{47, CDES70}$ -T relationship of Kele et al. (2015), produced
568 in the same laboratory and recalculated after Bernasconi et al. (2018). They determined that,
569 for a given temperature, dolomite- $\Delta_{47, CDES70}$ exceeded calcite- $\Delta_{47, CDES70}$ by ~30 ppm, a value
570 that exactly corresponded to the difference in $\Delta_{47, CDES70}^*$ between dolomite and calcite

571 observed by Müller et al. (2017). Their findings of inconsistent behavior between dolomite
572 and calcite were confirmed by Fosu et al. (2023), who modified the Kiel IV device to perform
573 90°C acid reactions. These authors, again, obtained significantly different calcite and dolomite
574 $\Delta_{47, I-CDES}$ -T relationships. In the most recent study of Anderson et al. (2024), dolomite
575 samples of controlled formation temperatures (25-1,200°C) were reacted at 70°C. As in the
576 study of Fosu et al. (2023), mass spectrometric raw data was corrected using IUPAC
577 parameters and calcite-based I-CDES standardization (Bernasconi et al., 2021). The
578 corresponding $\Delta_{47, I-CDES}$ -T relationship was indistinguishable from that of calcite after
579 Anderson et al. (2021) who reacted calcites at the same temperature and processed data the
580 same way as described in Anderson et al. (2024). Indirect evidence for calcite-like behavior of
581 dolomites is further given through a dual clumped isotope study focusing on paired calcite
582 and dolomite samples in an alteration setting (Lu et al., 2023).

583 Our dataset confirms previous studies that postulated the validity of a single Δ_{47} -T
584 relationship for both calcite and dolomite. Two dolomite calibration samples of Bonifacie et
585 al. (2017) are characterized by clumped isotope compositions that are indistinguishable
586 within their 2SEs from the calcite equilibrium relationship (Fiebig et al., 2024) (Figures 7a, b).
587 Moreover, $\Delta_{47, CDES90}$ values of 0.246 ± 0.008 ‰ (**Dolomite_350A-9**) and 0.593 ± 0.006 ‰
588 (**Dolomite_BE**), projected to the calcite equilibrium Δ_{47} -T relationship of Fiebig et al. (2024),
589 reflect temperatures of 344^{+29}_{-25} °C and $25.5^{+2.3}_{-2.2}$ °C, perfectly matching known formation
590 temperatures of 351.4 ± 2 °C and 25 ± 4 °C. On the contrary, sample **Dolomite_80-1**, which has
591 been precipitated through mixing of $MgSO_4$, $Ca(NO_3)_2 \cdot 4H_2O$, and Na_2CO_3 solutions at
592 80.2 ± 1 °C, deviates significantly from the calcite equilibrium line. It exhibits a relatively large
593 $+\Delta_{48}$ bias relative to its predicted equilibrium composition (Figure 9). It has been shown by
594 Hu et al. (2019), that nitrate, if present along with the carbonate, decomposes to NO_2 during
595 phosphoric acid digestion. Nitrate-derived NO_2 is not successfully removed from analyte CO_2
596 through gas purification, ultimately acting as isobaric interferent, thereby compromising Δ_{47}
597 and Δ_{48} values (Fiebig et al., 2024). Notably, the slope displayed by replicate Δ_{47}/Δ_{48} data of
598 **Dolomite_80-1** agrees within errors with the theoretical slope of -0.3 ± 0.05 indicative of NO_2
599 contamination (Figure 9). We therefore propose that this sample has been precipitated under
600 disequilibrium conditions and that its $\Delta_{47, CDES90}$ value fortuitously corresponded to a
601 temperature of 80°C when analyzed by Bonifacie et al. (2017). Notably, our $\Delta_{47, CDES90}$ value
602 of 0.468 ± 0.007 ‰ (fully propagated 2SE) obtained for this sample is identical to the
603 0.469 ± 0.009 ‰ (non-propagated, replicate-based 2SE) reported by Bonifacie et al. (2017),
604 implying that the degree of NO_2^+ contamination was comparable in the two analytical setups
605 used at GU and IPGP.
606



607
 608 Figure 9: Individual replicate $\Delta_{47, CDES90}$ and $\Delta_{48, CDES90}$ values (projected utilizing $\Delta_{47, 110-90^\circ C}^*$ and $\Delta_{48, 110-90^\circ C}^*$
 609 values of -0.0147 and -0.0148 ‰, respectively, see Table 3) for sample Dolomite_80-1 show significant
 610 correlation ($p=0.001$), sample mean value $\pm 2SEs$ displayed with black marker. The slope agrees within errors to
 611 that predicted for isobaric contamination through NO_2 (Fiebig et al., 2024). Back-extrapolating this vector
 612 intersects the equilibrium at a temperature of ca. $70^\circ C$, which is $10^\circ C$ colder than the precipitation temperature
 613 of ca. $80^\circ C$ (dotted horizontal line).

614 Dolomite samples of unknown formation temperatures (**D-Mio**, **IPGP-SRM88-1** and **IPGP-**
 615 **INYO**, Table 3) also plot indistinguishable from calcite Δ_{47}/Δ_{48} equilibrium (Figures 8a, b).
 616 Measured $\Delta_{47, CDES90}$ values for samples **D-Mio** reflect reasonable temperatures within the
 617 range $37-58^\circ C$, which are in accordance with the maximal temperature estimate of $60^\circ C$
 618 obtained through vitrinite reflectance measurements. The same applies to samples **IPGP-**
 619 **SRM88-1** and **IPGP-INYO** whose $\Delta_{47, CDES90}$ values indicate formation temperatures of
 620 $62.0^{+3.3}_{-3.1}^\circ C$ and $380^{+30.1}_{-25.8}^\circ C$, respectively.
 621 Taking into account that calcite and dolomite exhibit indistinguishable AFFs (Section 4.1), we
 622 suggest that calcite and dolomite also share $\Delta_{63}-T$ and $\Delta_{64}-T$ relationships. Accordingly, the
 623 equilibrium $\Delta_{47}-\Delta_{48}-1/T$ calibrations characteristic of calcite (Fiebig et al., 2021; 2024; Swart
 624 et al., 2021) can be applied to dolomite as well.

625 626 4.2.3 Witherite

627 There are several studies in which witherite was precipitated under controlled temperature
 628 conditions for clumped isotope analysis (e.g., Kong et al., 2023, Staudigel & Swart, 2018,
 629 Uchikawa et al., 2021). However, it should be noted that these publications precipitated the
 630 dissolved inorganic carbon (DIC) pool quantitatively, so that corresponding Δ_{47} values reflect
 631 DIC composition rather than witherite precipitated under equilibrium conditions. This most
 632 likely is the reason why e.g., the precipitates of Kong et al. (2023) have an average $+15$ ppm
 633 difference when compared to the calcite $\Delta_{47}-T$ relationship of Fiebig et al. (2024). Our low-
 634 temperature witherite sample, **DIC1**, which was precipitated from isotopically equilibrated
 635 solutions (5 % removal of DIC during precipitation), plots indistinguishably from dual clumped
 636 isotope equilibrium (Figure 7a). Its measured $\Delta_{47, CDES90}$ of 0.590 ± 0.007 ‰, projected to the
 637 calcite equilibrium $\Delta_{47}-T$ relationship of Fiebig et al. (2024), yields a temperature of $26.7^{+2.6}_{-2.6}^\circ C$
 638 that exactly confirms its known formation temperature of $25^\circ C$. This finding, along with our
 639 measured indistinguishable Δ_{47}^* and Δ_{48}^* AFFs for calcite and witherite (Section 4.1) strongly

640 implies that calcite and witherite share the same Δ_{47} -T and Δ_{48} -T equilibrium relationships
641 over the entire temperature range from 25-1100°C. Because differences in Δ_{47}^* , Δ_{48}^* , Δ_{47} -T
642 and Δ_{48} -T between calcite and witherite are insignificant, it follows that Δ_{63} -T and Δ_{64} -T
643 relationships are also identical.

644

645 4.2.4 Siderite

646 Fernandez et al. (2014) reacted siderite and calcite formed at known temperatures at 100°C
647 and could not resolve any significant differences in corresponding Δ_{47} -T relationships. In the
648 most recent study of Holme et al. (2023), siderite was reacted at 90°C. These authors
649 observed that their apparent Δ_{47} -T relationship for pure siderite departed by -20 ppm from
650 the composite Δ_{47} -T calcite calibration of Petersen et al. (2019) which considered
651 synthetically precipitated calcite (Defliese et al., 2015; Kelson et al., 2017; Kluge et al., 2015;
652 Passey & Henkes, 2012; Tang et al., 2014), aragonite (Defliese et al., 2015; Kelson et al., 2017;
653 Kluge et al., 2015), dolomite (Winkelstern et al., 2016), and siderite (Fernandez et al., 2014).
654 For a given temperature, Petersen et al. (2019) did not find any significant differences in Δ_{47}
655 values between all these mineralogies when all original data was reprocessed using IUPAC
656 parameters. A systematic offset to lower Δ_{47} values, however, was also observed by van Dijk
657 et al. (2019) when comparing their siderite- $\Delta_{47, CDES70}$ values to those obtained on calcite and
658 aragonite presented by Kele et al. (2015). Van Dijk et al. (2019) attributed the observed
659 discrepancy to differences in the acid fractionation factor between siderite and
660 aragonite/calcite. This interpretation was not supported by the data of Holme et al. (2023),
661 who explained the observed offset of siderite Δ_{47} with respect to calcite with
662 supersaturation-related kinetic isotope effects being recorded in siderite.

663 After correction for calcite-specific $\Delta_{47, 110-90^\circ C}^*$ and $\Delta_{48, 110-90^\circ C}^*$ values, $\Delta_{47, CDES90}$ and
664 $\Delta_{48, CDES90}$ values of CO₂ extracted from our natural siderite samples **Sid_D1-Sid_D6** at 110°C
665 (Section 3.3) are within error, indistinguishable from the proposed calcite equilibrium
666 relationship (Fiebig et al., 2024) (Figure 8a). The dual clumped isotope composition of IPGPs
667 internal siderite standard, **IPGP-SID1**, also falls on the calcite equilibrium line (Figure 8b). Its
668 $\Delta_{47, CDES90}$ -derived temperature is 213_{-9}^{+10} °C. At a first glance, these results, therefore, do
669 support previous findings according to which siderite and calcite are characterized by
670 identical equilibrium Δ_{47} -T relationships (e.g., Fernandez et al., 2014; Petersen et al., 2019).
671 However, in our case, formation temperatures and conditions (e.g., precipitation rates) of
672 investigated siderites are unknown. We, therefore, cannot rule out that their dual clumped
673 compositions were biased by kinetics and only fortuitously correspond to equilibrium. In any
674 case, more analyses on siderites precipitated under controlled conditions, devoid of kinetic
675 bias, are necessary to evaluate with more confidence if siderite and calcite are characterized
676 by a common Δ_{47} - Δ_{48} -T relationship.

677

678 5. Conclusions

679 We have investigated the dual clumped isotope compositions of stochastic and low-
680 temperature samples of calcite, aragonite, dolomite, witherite and siderite at acid digestion
681 temperatures of 90 and 110°C. Data projected to the CDES90 shows no significant differences
682 in acid fractionation factors between investigated mineralogies. $\Delta_{47, CDES90}$ values of low-
683 temperature samples of aragonite, dolomite, witherite and siderite plot indistinguishably
684 from the equilibrium calcite $\Delta_{47}-\Delta_{48}-T$ relationship of Fiebig et al. (2021) revised after Fiebig
685 et al. (2024), and $\Delta_{47, CDES90}$ values of aragonite, dolomite and witherite samples exactly
686 confirm known formation temperatures. These results demonstrate that a single $\Delta_{47}-\Delta_{48}-T$
687 relationship is valid for calcite, aragonite, dolomite and witherite. We do not have any
688 indication that this relationship might not be applicable to siderite, however high-precision
689 data on siderites precipitated under controlled conditions is necessary to confirm this
690 hypothesis. The universal application of calcite-specific $\Delta_{47}-\Delta_{48}-T$ relationships to aragonite,
691 dolomite and witherite provides a promising framework for consistent isotopic analyses in
692 different carbonate samples. These results have significant implications for improving the
693 accuracy of temperature reconstructions in paleoenvironmental studies.

694

695 Acknowledgements

696 J.F. acknowledges funding through DFG, Reinhart Koselleck project FI-948/13-1 and E.H.
697 acknowledges DFG funding HA-5137/5. Sven Hofmann is acknowledged for technical support.
698 We would like to thank Vanessa Schlidt, Amelia Davies, Mattia Tagliavento,
699 Manuel Schumann, Phil Dolz and Armelle Ballian for assistance in the clumped isotope
700 laboratory. We thank Niels de Winter and Vanessa Schlidt for providing samples AI_006 and
701 RM1, respectively. Juske Horita is acknowledged for providing (proto)dolomites. We
702 acknowledge Karel Mach, Chief Geologist at the Bilina Mine, for providing siderite material.

703

704 CRedit statement

705 **Bernecker Miguel:** Methodology, Software, Validation, Formal analysis, Investigation, Data
706 Curation, Writing - Original Draft, Writing - Review & Editing, Visualization, Supervision,
707 Project administration, Funding acquisition. **Bonifacie Magali:** Conceptualization,
708 Methodology, Resources, Writing - Review & Editing, Project administration. **Staudigel Philip:**
709 Investigation, Writing - Review & Editing. **Meijer Niels:** Investigation, Writing - Review &
710 Editing. **Siebert Julien:** Investigation. **Wehr Nicolas:** Investigation. **Haussühl Eiken:**
711 Investigation, Writing - Review & Editing, Funding acquisition. **Bernasconi Stefano M.:**
712 Resources, Writing - Review & Editing. **Petrash Daniel:** Resources, Writing - Review & Editing.
713 **Dietzel Martin:** Resources. **Fiebig Jens:** Conceptualization, Methodology, Investigation,
714 Writing - Original Draft, Writing - Review & Editing, Supervision, Project administration,
715 Funding acquisition.

716

717 Appendix A. Supplementary Material

718 Clumped isotope data utilized for this manuscript can be found in Supplementary Materials S1
719 and S2 (spreadsheets). Supplementary Materials S1 keeps the mass-spectrometric input data
720 as pre-processed δ^{45} - δ^{49} values, which were determined from baseline-corrected raw data.
721 Clumped isotope processing result containing replicate-level results, a sample overview
722 summary, as well as session-wise standardization parameters and statistics are stored in
723 Supplementary Material S2. X-ray diffractograms for our thermally re-ordered samples and
724 DIC1 (Section 3.1) are available from Supplementary Material S3 (document).
725

726 Data Availability

727 Research data are available from <https://doi.org/10.5281/zenodo.14843259>, and from the
728 Supplementary Materials S1 and S2.
729

730 References

- 731 Anderson, N. T., Bonifacie, M., Jost, A. B., Siebert, J., Bontognali, T., Horita, J., Müller, I. A.,
732 Bernasconi, S. M., & Bergmann, K. D. (2024). Re-Assessing the Need for Apatite- and
733 Dolomite-Specific Calibrations of the Carbonate Clumped Isotope Thermometer.
734 *Geochemistry, Geophysics, Geosystems*, 25(1). <https://doi.org/10.1029/2023GC011049>
735 Arndt, I., Bernecker, M., Erhardt, T., Evans, D., Fiebig, J., Fursman, M., Kniest, J., Renema, W.,
736 Schlidt, V., Staudigel, P., Voigt, S., & Müller, W. (2025). 20,000 days in the life of a giant
737 clam reveal late Miocene tropical climate variability. *Palaeogeography,*
738 *Palaeoclimatology, Palaeoecology*, 661. <https://doi.org/10.1016/j.palaeo.2024.112711>
739 Bajnai, D., Guo, W., Spötl, C., Coplen, T. B., Methner, K., Löffler, N., Krsnik, E., Gischler, E.,
740 Hansen, M., Henkel, D., Price, G. D., Raddatz, J., Scholz, D., & Fiebig, J. (2020). Dual
741 clumped isotope thermometry resolves kinetic biases in carbonate formation
742 temperatures. *Nature Communications*, 11(1). [https://doi.org/10.1038/s41467-020-](https://doi.org/10.1038/s41467-020-17501-0)
743 [17501-0](https://doi.org/10.1038/s41467-020-17501-0)
744 Bernasconi, S. M., Daëron, M., Bergmann, K. D., Bonifacie, M., Meckler, A. N., Affek, H. P.,
745 Anderson, N., Bajnai, D., Barkan, E., Beverly, E., Blamart, D., Burgener, L., Calmels, D.,
746 Chaduteau, C., Clog, M., Davidheiser-Kroll, B., Davies, A., Dux, F., Eiler, J., ... Ziegler, M.
747 (2021). InterCarb: A Community Effort to Improve Interlaboratory Standardization of the
748 Carbonate Clumped Isotope Thermometer Using Carbonate Standards. *Geochemistry,*
749 *Geophysics, Geosystems*, 22(5). <https://doi.org/10.1029/2020GC009588>
750 Bernasconi, S. M., Müller, I. A., Bergmann, K. D., Breitenbach, S. F. M., Fernandez, A., Hodell,
751 D. A., Jaggi, M., Meckler, A. N., Millan, I., & Ziegler, M. (2018). Reducing Uncertainties in
752 Carbonate Clumped Isotope Analysis Through Consistent Carbonate-Based
753 Standardization. *Geochemistry, Geophysics, Geosystems*, 19(9), 2895–2914.
754 <https://doi.org/10.1029/2017GC007385>
755 Bernecker, M., Hofmann, S., Staudigel, P. T., Davies, A. J., Tagliavento, M., Meijer, N., Ballian,
756 A., & Fiebig, J. (2023). A robust methodology for triple ($\Delta 47$, $\Delta 48$, $\Delta 49$) clumped isotope
757 analysis of carbonates. *Chemical Geology*, 642, 121803.
758 <https://doi.org/10.1016/j.chemgeo.2023.121803>
759 Bigeleisen, J. (1965). Chemistry of Isotopes. *Science*, 147(3657), 463–471.
760 <https://doi.org/10.1126/science.147.3657.463>

761 Bonifacie, M., Calmels, D., Eiler, J. M., Horita, J., Chaduteau, C., Vasconcelos, C., Agrinier, P.,
762 Katz, A., Passey, B. H., Ferry, J. M., & Bourrand, J. J. (2017). Calibration of the dolomite
763 clumped isotope thermometer from 25 to 350 °C, and implications for a universal
764 calibration for all (Ca, Mg, Fe)CO₃ carbonates. *Geochimica et Cosmochimica Acta*, 200,
765 255–279. <https://doi.org/10.1016/j.gca.2016.11.028>

766 Böttcher, M. E. (1996). 18O/16O and 13C/12C fractionation during the reaction of carbonates
767 with phosphoric acid effects of cationic substitution and reaction temperature. *Isotopes*
768 *in Environmental and Health Studies*, 32(2–3), 299–305.
769 <https://doi.org/10.1080/10256019608036323>

770 Came, R. E., Eiler, J. M., Veizer, J., Azmy, K., Brand, U., & Weidman, C. R. (2007). Coupling of
771 surface temperatures and atmospheric CO₂ concentrations during the Palaeozoic era.
772 *Nature*, 449(7159), 198–201. <https://doi.org/10.1038/nature06085>

773 Crouzet, C., Brunet, F., Recham, N., Findling, N., Lanson, M., Guyot, F., Ferrasse, J. H., & Goffé,
774 B. (2017). Hydrogen production by hydrothermal oxidation of FeO under acidic
775 conditions. *International Journal of Hydrogen Energy*, 42(2), 795–806.
776 <https://doi.org/10.1016/j.ijhydene.2016.10.019>

777 Daëron, M. (2021). Full Propagation of Analytical Uncertainties in $\Delta 47$ Measurements.
778 *Geochemistry, Geophysics, Geosystems*, 22(5). <https://doi.org/10.1029/2020GC009592>

779 Daëron, M., Blamart, D., Peral, M., & Affek, H. P. (2016). Absolute isotopic abundance ratios
780 and the accuracy of $\Delta 47$ measurements. *Chemical Geology*, 442, 83–96.
781 <https://doi.org/10.1016/j.chemgeo.2016.08.014>

782 Daëron, M., & Vermeesch, P. (2024). Omnivariant Generalized Least Squares regression:
783 Theory, geochronological applications, and making the case for reconciled $\Delta 47$
784 calibrations. *Chemical Geology*, 647. <https://doi.org/10.1016/j.chemgeo.2023.121881>

785 Davies, A. J., Brand, U., Tagliavento, M., Bitner, M. A., Bajnai, D., Staudigel, P., Bernecker, M.,
786 & Fiebig, J. (2023). Isotopic disequilibrium in brachiopods disentangled with dual
787 clumped isotope thermometry. *Geochimica et Cosmochimica Acta*.
788 <https://doi.org/10.1016/j.gca.2023.08.005>

789 Davies, A. J., Guo, W., Bernecker, M., Tagliavento, M., Raddatz, J., Gischler, E., Flögel, S., &
790 Fiebig, J. (2022). Dual clumped isotope thermometry of coral carbonate. *Geochimica et*
791 *Cosmochimica Acta*, 338, 66–78. <https://doi.org/10.1016/j.gca.2022.10.015>

792 de Winter, N. J., Witbaard, R., Kocken, I. J., Müller, I. A., Guo, J., Goudsmit, B., & Ziegler, M.
793 (2022). Temperature Dependence of Clumped Isotopes ($\Delta 47$) in Aragonite. *Geophysical*
794 *Research Letters*, 49(20). <https://doi.org/10.1029/2022GL099479>

795 Defliese, W. F., Hren, M. T., & Lohmann, K. C. (2015). Compositional and temperature effects
796 of phosphoric acid fractionation on $\delta 47$ analysis and implications for discrepant
797 calibrations. *Chemical Geology*, 396, 51–60.
798 <https://doi.org/10.1016/j.chemgeo.2014.12.018>

799 Dennis, K. J., Affek, H. P., Passey, B. H., Schrag, D. P., & Eiler, J. M. (2011). Defining an absolute
800 reference frame for ‘clumped’ isotope studies of CO₂. *Geochimica et Cosmochimica*
801 *Acta*, 75(22), 7117–7131. <https://doi.org/10.1016/j.gca.2011.09.025>

802 Fernandez, A., Tang, J., & Rosenheim, B. E. (2014). Siderite ‘clumped’ isotope thermometry:
803 A new paleoclimate proxy for humid continental environments. *Geochimica et*
804 *Cosmochimica Acta*, 126, 411–421. <https://doi.org/10.1016/j.gca.2013.11.006>

805 Fiebig, J., Bajnai, D., Löffler, N., Methner, K., Krsnik, E., Mulch, A., & Hofmann, S. (2019).
806 Combined high-precision $\Delta 48$ and $\Delta 47$ analysis of carbonates. *Chemical Geology*, 522,
807 186–191. <https://doi.org/10.1016/j.chemgeo.2019.05.019>

808 Fiebig, J., Bernecker, M., Meijer, N., Methner, K., Staudigel, P., Davies, A. J., Bayarjargal, L.,
809 Spahr, D., Winkler, B., Hofmann, S., Granzin, M., & Petersen, S. V. (2024). Carbonate
810 clumped isotope values compromised by nitrate-derived NO₂ interferent. *Chemical*
811 *Geology*, 122382. <https://doi.org/10.1016/j.chemgeo.2024.122382>

812 Fiebig, J., Daëron, M., Bernecker, M., Guo, W., Schneider, G., Boch, R., Bernasconi, S. M.,
813 Jautzy, J., & Dietzel, M. (2021). Calibration of the dual clumped isotope thermometer for
814 carbonates. *Geochimica et Cosmochimica Acta*.
815 <https://doi.org/10.1016/j.gca.2021.07.012>

816 Fiebig, J., Hofmann, S., Löffler, N., Lüdecke, T., Methner, K., & Wacker, U. (2016). Slight
817 pressure imbalances can affect accuracy and precision of dual inlet-based clumped
818 isotope analysis. *Isotopes in Environmental and Health Studies*, 52(1–2), 12–28.
819 <https://doi.org/10.1080/10256016.2015.1010531>

820 Fosu, B. R., Jautzy, J. J., Yong, W., & Secco, R. A. (2023). Introducing the “Franken-Kiel”
821 Carbonate Device: First Application to $\Delta 47$ -T Calibrations of Calcite and Dolomite.
822 *Geochemistry, Geophysics, Geosystems*, 24(10). <https://doi.org/10.1029/2023GC011047>

823 Ghosh, P., Adkins, J., Affek, H., Balta, B., Guo, W., Schauble, E. A., Schrag, D., & Eiler, J. M.
824 (2006). ^{13}C - ^{18}O bonds in carbonate minerals: A new kind of paleothermometer.
825 *Geochimica et Cosmochimica Acta*, 70(6), 1439–1456.
826 <https://doi.org/10.1016/j.gca.2005.11.014>

827 Ghosh, P., Eiler, J., Campana, S. E., & Feeney, R. F. (2007). Calibration of the carbonate
828 ‘clumped isotope’ paleothermometer for otoliths. *Geochimica et Cosmochimica Acta*,
829 71(11), 2736–2744. <https://doi.org/10.1016/j.gca.2007.03.015>

830 Gilg, H. A., Struck, U., Vennemann, T., & Boni, M. (2003). Phosphoric acid fractionation factors
831 for smithsonite and cerussite between 25 and 72°C. *Geochimica et Cosmochimica Acta*,
832 67(21), 4049–4055. [https://doi.org/10.1016/S0016-7037\(03\)00169-8](https://doi.org/10.1016/S0016-7037(03)00169-8)

833 Guo, W., Mosenfelder, J. L., Goddard, W. A., & Eiler, J. M. (2009). Isotopic fractionations
834 associated with phosphoric acid digestion of carbonate minerals: Insights from first-
835 principles theoretical modeling and clumped isotope measurements. *Geochimica et*
836 *Cosmochimica Acta*, 73(24), 7203–7225. <https://doi.org/10.1016/j.gca.2009.05.071>

837 Henkes, G. A., Passey, B. H., Wanamaker, A. D., Grossman, E. L., Ambrose, W. G., & Carroll, M.
838 L. (2013). Carbonate clumped isotope compositions of modern marine mollusk and
839 brachiopod shells. *Geochimica et Cosmochimica Acta*, 106, 307–325.
840 <https://doi.org/10.1016/j.gca.2012.12.020>

841 Holme, E. A., Henkes, G. A., Tosca, N. J., Rasbury, E. T., Young, J. M., Schaub, D. R., Nekvasil,
842 H., & Hurowitz, J. A. (2023). Experimental constraints on siderite clumped isotope
843 thermometry. *Geochimica et Cosmochimica Acta*, 343, 323–340.
844 <https://doi.org/10.1016/j.gca.2022.12.012>

845 Horita, J. (2014). Oxygen and carbon isotope fractionation in the system dolomite-water-CO₂
846 to elevated temperatures. *Geochimica et Cosmochimica Acta*, 129, 111–124.
847 <https://doi.org/10.1016/j.gca.2013.12.027>

848 Hu, B., Gao, J., Fan, C., Li, Y., Qin, Y., Zhao, Y., & Tian, Y. (2019). Impact of nitrate contamination
849 on the analysis of carbon and oxygen isotopes in carbonate and a low-temperature
850 phosphoric acid digestion approach for online sample preparation. *Rapid*
851 *Communications in Mass Spectrometry*, 33(1), 12–20. <https://doi.org/10.1002/rcm.8289>

852 Kele, S., Breitenbach, S. F. M., Capezzuoli, E., Meckler, A. N., Ziegler, M., Millan, I. M., Kluge,
853 T., Deák, J., Hanselmann, K., John, C. M., Yan, H., Liu, Z., & Bernasconi, S. M. (2015).
854 Temperature dependence of oxygen- and clumped isotope fractionation in carbonates:

855 A study of travertines and tufas in the 6–95°C temperature range. *Geochimica et*
856 *Cosmochimica Acta*, 168, 172–192. <https://doi.org/10.1016/j.gca.2015.06.032>

857 Kelson, J. R., Huntington, K. W., Schauer, A. J., Saenger, C., & Lechler, A. R. (2017). Toward a
858 universal carbonate clumped isotope calibration: Diverse synthesis and preparatory
859 methods suggest a single temperature relationship. *Geochimica et Cosmochimica Acta*,
860 197, 104–131. <https://doi.org/10.1016/j.gca.2016.10.010>

861 Kim, S. T., O’Neil, J. R., Hillaire-Marcel, C., & Mucci, A. (2007). Oxygen isotope fractionation
862 between synthetic aragonite and water: Influence of temperature and Mg²⁺
863 concentration. *Geochimica et Cosmochimica Acta*, 71(19), 4704–4715.
864 <https://doi.org/10.1016/j.gca.2007.04.019>

865 Kim, S.-T., & O’Neil, J. R. (1997). Equilibrium and nonequilibrium oxygen isotope effects in
866 synthetic carbonates. *Geochimica et Cosmochimica Acta*, 61(16), 3461–3475.
867 [https://doi.org/10.1016/S0016-7037\(97\)00169-5](https://doi.org/10.1016/S0016-7037(97)00169-5)

868 Kluge, T., John, C. M., Jourdan, A. L., Davis, S., & Crawshaw, J. (2015). Laboratory calibration
869 of the calcium carbonate clumped isotope thermometer in the 25–250°C temperature
870 range. *Geochimica et Cosmochimica Acta*, 157, 213–227.
871 <https://doi.org/10.1016/j.gca.2015.02.028>

872 Kniest, J. F., Davies, A. J., Brugger, J., Fiebig, J., Bernecker, M., Todd, J. A., Hickler, T., Voigt, S.,
873 Woodland, A., & Raddatz, J. (2024). Dual clumped isotopes from Mid-Eocene bivalve
874 shell reveal a hot and summer wet climate of the Paris Basin. *Communications Earth and*
875 *Environment*, 5(1). <https://doi.org/10.1038/s43247-024-01491-8>

876 Kong, K., Guo, Y., Deng, W., & Wei, G. (2023). Synthetic Witherite for Standardisation of
877 Clumped Isotope ($\Delta 47$) Measurements. *Geostandards and Geoanalytical Research*,
878 47(4), 855–868. <https://doi.org/10.1111/ggr.12520>

879 Kříbek, B., Knésl, I., Rojík, P., Sýkorová, I., & Martínek, K. (2017). Geochemical history of a
880 Lower Miocene lake, the Cypris Formation, Sokolov Basin, Czech Republic. *Journal of*
881 *Paleolimnology*, 58(2), 169–190. <https://doi.org/10.1007/s10933-017-9970-2>

882 Kruskal, W. H., & Wallis, W. A. (1952). Use of Ranks in One-Criterion Variance Analysis. In
883 *Source: Journal of the American Statistical Association* (Vol. 47, Issue 260).

884 Lafuente, B., Downs, R. T., Yang, H., & Stone, N. (2015). 1. The power of databases: The RRUFF
885 project. In *Highlights in Mineralogical Crystallography* (pp. 1–30). DE GRUYTER.
886 <https://doi.org/10.1515/9783110417104-003>

887 Lebeau, O., Busigny, V., Chaduteau, C., & Ader, M. (2014). Organic matter removal for the
888 analysis of carbon and oxygen isotope compositions of siderite. *Chemical Geology*, 372,
889 54–61. <https://doi.org/10.1016/j.chemgeo.2014.02.020>

890 Lu, C., Murray, S. T., Klaus, J., McNeill, D. F., & Swart, P. K. (2024). Dual clumped isotopes ($\Delta 47$
891 and $\Delta 48$) reveal non-equilibrium formation of freshwater cements. *Geochimica et*
892 *Cosmochimica Acta*, 379, 145–157. <https://doi.org/10.1016/j.gca.2024.06.037>

893 Lu, C., Zou, H., Wang, G., Cong, F., Quan, Y., & Swart, P. K. (2023). Clumped isotopes of paired
894 dolomite and calcite constraining alteration histories of ancient carbonate successions.
895 *Chemical Geology*, 617. <https://doi.org/10.1016/j.chemgeo.2022.121264>

896 Mann, H. B., & Whitney, D. R. (1947). On a Test of Whether one of Two Random Variables is
897 Stochastically Larger than the Other. *The Annals of Mathematical Statistics*, 18(1), 50–
898 60. <https://doi.org/10.1214/aoms/1177730491>

899 McCrea, J. M. (1950). On the isotopic chemistry of carbonates and a paleotemperature scale.
900 *The Journal of Chemical Physics*, 18(6), 849–857. <https://doi.org/10.1063/1.1747785>

901 Müller, I. A., Rodriguez-Blanco, J. D., Storck, J. C., do Nascimento, G. S., Bontognali, T. R. R.,
902 Vasconcelos, C., Benning, L. G., & Bernasconi, S. M. (2019). Calibration of the oxygen and
903 clumped isotope thermometers for (proto-)dolomite based on synthetic and natural
904 carbonates. *Chemical Geology*, 525, 1–17.
905 <https://doi.org/10.1016/j.chemgeo.2019.07.014>

906 Müller, I. A., Violay, M. E. S., Storck, J. C., Fernandez, A., van Dijk, J., Madonna, C., &
907 Bernasconi, S. M. (2017). Clumped isotope fractionation during phosphoric acid
908 digestion of carbonates at 70 °C. *Chemical Geology*, 449, 1–14.
909 <https://doi.org/10.1016/j.chemgeo.2016.11.030>

910 Parvez, Z. A., Lucarelli, J. K., Matamoros, I. W., Rubi, J., Miguel, K., Elliott, B., Flores, R., Ulrich,
911 R. N., Eagle, R. A., Watkins, J. M., Christensen, J. N., & Tripathi, A. (2023). Dual carbonate
912 clumped isotopes ($\Delta 47$ - $\Delta 48$) constrains kinetic effects and timescales in peridotite-
913 associated springs at the Cedars, Northern California. *Geochimica et Cosmochimica Acta*,
914 358, 77–92. <https://doi.org/10.1016/j.gca.2023.06.022>

915 Passey, B. H., & Henkes, G. A. (2012). Carbonate clumped isotope bond reordering and
916 geospeedometry. *Earth and Planetary Science Letters*, 351–352, 223–236.
917 <https://doi.org/10.1016/j.epsl.2012.07.021>

918 Passey, B. H., Levin, N. E., Cerling, T. E., Brown, F. H., & Eiler, J. M. (2010). High-temperature
919 environments of human evolution in East Africa based on bond ordering in paleosol
920 carbonates. *Proceedings of the National Academy of Sciences of the United States of*
921 *America*, 107(25), 11245–11249. <https://doi.org/10.1073/pnas.1001824107>

922 Petersen, S. V., Defliese, W. F., Saenger, C., Daëron, M., Huntington, K. W., John, C. M., Kelson,
923 J. R., Bernasconi, S. M., Colman, A. S., Kluge, T., Olack, G. A., Schauer, A. J., Bajnai, D.,
924 Bonifacie, M., Breitenbach, S. F. M., Fiebig, J., Fernandez, A. B., Henkes, G. A., Hodell, D.,
925 ... Winkelstern, I. Z. (2019). Effects of Improved ^{17}O Correction on Interlaboratory
926 Agreement in Clumped Isotope Calibrations, Estimates of Mineral-Specific Offsets, and
927 Temperature Dependence of Acid Digestion Fractionation. *Geochemistry, Geophysics,*
928 *Geosystems*, 20(7), 3495–3519. <https://doi.org/10.1029/2018GC008127>

929 Rojik, P. (2004). Journal of geosciences. *Journal of the Czech Geological Society*, 49(3–4), 173–
930 185. <http://www.jgeosci.org/detail/JCGS.969>

931 Rosenbaum, J., & Sheppard, S. M. F. (1986). An isotopic study of siderites, dolomites and
932 ankerites at high temperatures. *Geochimica et Cosmochimica Acta*, 50(6), 1147–1150.
933 [https://doi.org/10.1016/0016-7037\(86\)90396-0](https://doi.org/10.1016/0016-7037(86)90396-0)

934 Schauble, E. A., Ghosh, P., & Eiler, J. M. (2006). Preferential formation of ^{13}C - ^{18}O bonds in
935 carbonate minerals, estimated using first-principles lattice dynamics. *Geochimica et*
936 *Cosmochimica Acta*, 70(10), 2510–2529. <https://doi.org/10.1016/j.gca.2006.02.011>

937 Schauer, A. J., Kelson, J., Saenger, C., & Huntington, K. W. (2016). Choice of ^{17}O correction
938 affects clumped isotope ($\Delta 47$) values of CO_2 measured with mass spectrometry. *Rapid*
939 *Communications in Mass Spectrometry*, 30(24), 2607–2616.
940 <https://doi.org/10.1002/rcm.7743>

941 Sharma, T., & Clayton, R. N. (1965). Measurement of ratios of total oxygen of carbonates.
942 *Geochimica et Cosmochimica Acta*, 29(12), 1347–1353. [https://doi.org/10.1016/0016-7037\(65\)90011-6](https://doi.org/10.1016/0016-7037(65)90011-6)

943

944 Siebert, J., Corgne, A., & Ryerson, F. J. (2011). Systematics of metal-silicate partitioning for
945 many siderophile elements applied to Earth's core formation. *Geochimica et*
946 *Cosmochimica Acta*, 75(6), 1451–1489. <https://doi.org/10.1016/j.gca.2010.12.013>

947 Staudigel, P., Feng, D., Peckmann, J., Bernecker, M., Davies, A., Tagliavento, M., & Fiebig, J.
948 (2024). Resolving and correcting for kinetic biases on methane seep paleotemperature
949 using carbonate Δ_{47}/Δ_{48} analysis. *Science Advances*, *10*(22), 155.
950 <https://doi.org/10.1126/sciadv.adn0155>

951 Staudigel, P. T., & Swart, P. K. (2018). A Kinetic Difference Between 12C- and 13C-Bound
952 Oxygen Exchange Rates Results in Decoupled $\delta^{18}O$ and Δ_{47} Values of Equilibrating DIC
953 Solutions. *Geochemistry, Geophysics, Geosystems*, *19*(8), 2371–2383.
954 <https://doi.org/10.1029/2018GC007500>

955 Swart, P. K., Burns, S. J., & Leder, J. J. (1991). Fractionation of the stable isotopes of oxygen
956 and carbon in carbon dioxide during the reaction of calcite with phosphoric acid as a
957 function of temperature and technique. *Chemical Geology: Isotope Geoscience Section*,
958 *86*(2), 89–96. [https://doi.org/10.1016/0168-9622\(91\)90055-2](https://doi.org/10.1016/0168-9622(91)90055-2)

959 Tagliavento, M., Davies, A. J., Bernecker, M., Staudigel, P. T., Dawson, R. R., Dietzel, M.,
960 Götschl, K., Guo, W., Schulp, A. S., Therrien, F., Zelenitsky, D. K., Gerdes, A., Müller, W.,
961 & Fiebig, J. (2023). Evidence for heterothermic endothermy and reptile-like eggshell
962 mineralization in Troodon, a non-avian maniraptoran theropod. *Proceedings of the
963 National Academy of Sciences of the United States of America*, *120*(15).
964 <https://doi.org/10.1073/pnas.2213987120>

965 Tang, J., Dietzel, M., Fernandez, A., Tripathi, A. K., & Rosenheim, B. E. (2014). Evaluation of
966 kinetic effects on clumped isotope fractionation (δ_{47}) during inorganic calcite
967 precipitation. *Geochimica et Cosmochimica Acta*, *134*, 120–136.
968 <https://doi.org/10.1016/j.gca.2014.03.005>

969 Tripathi, A. K., Eagle, R. A., Thiagarajan, N., Gagnon, A. C., Bauch, H., Halloran, P. R., & Eiler, J.
970 M. (2010). 13C-18O isotope signatures and ‘clumped isotope’ thermometry in
971 foraminifera and coccoliths. *Geochimica et Cosmochimica Acta*, *74*(20), 5697–5717.
972 <https://doi.org/10.1016/j.gca.2010.07.006>

973 Tripathi, A. K., Hill, P. S., Eagle, R. A., Mosenfelder, J. L., Tang, J., Schauble, E. A., Eiler, J. M.,
974 Zeebe, R. E., Uchikawa, J., Coplen, T. B., Ries, J. B., & Henry, D. (2015). Beyond
975 temperature: Clumped isotope signatures in dissolved inorganic carbon species and the
976 influence of solution chemistry on carbonate mineral composition. *Geochimica et
977 Cosmochimica Acta*, *166*, 344–371. <https://doi.org/10.1016/j.gca.2015.06.021>

978 Uchikawa, J., Chen, S., Eiler, J. M., Adkins, J. F., & Zeebe, R. E. (2021). Trajectory and timescale
979 of oxygen and clumped isotope equilibration in the dissolved carbonate system under
980 normal and enzymatically-catalyzed conditions at 25 °C. *Geochimica et Cosmochimica
981 Acta*, *314*, 313–333. <https://doi.org/10.1016/j.gca.2021.08.014>

982 Urey, H. C. (1947). The thermodynamic properties of isotopic substances. *Journal of the
983 Chemical Society (Resumed)*, 562. <https://doi.org/10.1039/jr9470000562>

984 Wacker, U., Fiebig, J., & Schoene, B. R. (2013). Clumped isotope analysis of carbonates:
985 comparison of two different acid digestion techniques. *Rapid Communications in Mass
986 Spectrometry*, *27*(14), 1631–1642. <https://doi.org/10.1002/rcm.6609>

987 Walters, L. J., Claypool, G. E., & Choquette, P. W. (1972). Reaction rates and SO_1^* variation
988 for the carbonate-phosphoric acid preparation method. *Geochimica et Cosmochimica
989 Acta*, *36*, 129–140.

990 Wang, Z., Schauble, E. A., & Eiler, J. M. (2004). Equilibrium thermodynamics of multiply
991 substituted isotopologues of molecular gases. *Geochimica et Cosmochimica Acta*, *68*(23),
992 4779–4797. <https://doi.org/10.1016/j.gca.2004.05.039>

- 993 Wendeberg, M., Richter, J. M., Rothe, M., & Brand, W. A. (2011). $\delta^{18}\text{O}$ anchoring to VPDB:
994 Calcite digestion with ^{18}O -adjusted ortho-phosphoric acid. *Rapid Communications in*
995 *Mass Spectrometry*, 25(7), 851–860. <https://doi.org/10.1002/rcm.4933>
- 996 Winkelstern, I. Z., Kaczmarek, S. E., Lohmann, K. C., & Humphrey, J. D. (2016). Calibration of
997 dolomite clumped isotope thermometry. *Chemical Geology*, 443, 32–38.
998 <https://doi.org/10.1016/j.chemgeo.2016.09.021>
- 999 Zimmerman, D. W. (2000). Statistical significance levels of nonparametric tests biased by
1000 heterogeneous variances of treatment groups. *Journal of General Psychology*, 127(4),
1001 354–364. <https://doi.org/10.1080/00221300009598589>
1002